90 p.

NASA Contractor Report 179472

IN-14859

Determination of Solid Mass Fraction in Partially Frozen Hydrocarbon Fuels

E.M. Cotterell, R. Mossadegh,
A.J. Bruce, and C.T. Moynihan

Rensselaer Polytechnic Institute
Troy, New York

July 1986

Prepared for
Lewis Research Center
Under Grant NAG 3-213

National Aeronautics and
Space Administration

CONTENTS

1. INTRODUCTION

As demand for petroleum fractions in the medium distillate fuel range increases, the need for alternative hydrocarbon sources and increased consumption of conventional crudes will also increase. This trend will likely be accompanied by relaxation of some fuel specifications. Of particular interest in jet fuel applications is the maximum allowed freezing point, which is set to ensure flowability of the fuel in the low temperature conditions experienced during high altitude flight.

To achieve optimum usage of such fuels it is important to be able to characterize their freezing behavior. To date, thermal and compositional studies as well as environmental simulations have been conducted in response to this concern.

Hydrocarbon fuels contain many components and freeze over a wide temperature range. Their low temperature properties are therefore not adequately defined by one parameter and several ASTM tests are typically used. These include: Cloud Point, Freeze Point, Wax Appearance Point, and Pour Point [1].

Cloud Point, ASTM D 2500-66, is the temperature at which, when cooled, a haze of crystals can first be seen at the bottom of the test jar. Freeze Point, ASTM D 2386-67, is the temperature at which crystals formed on cooling disappear when the fuel is subsequently reheated. Note that this method actually defines the liquidus temperature and henceforth will be referred to as the ASTM Melting Point. Wax Appearance Point, ASTM D 3117-72, is the temperature at which a "swirl" of wax crystals around the stirrer is first observed

under prescribed cooling conditions. Pour Point, ASTM D 97-66, is the temperature 5 °F above that at which the surface of a partly frozen fuel is first observed not to move when held in a horizontal position, also under prescribed quick-cooling conditions.

Each of these tests is aimed at locating a particular extent of freezing. In conjunction with this information it is useful to know the mass fraction of crystallizing solid as a function of temperature. This can be done with a filtration procedure which is augmented by an independent spectrophotometric determination of concentrations of tracer dyes in the separated liquid and solid fractions to determine the large amount of liquid which is entrapped within the filtered crystalline solid [2].

In this study, we have modified and improved this technique for determining the mass fraction of crystallized solids in the following ways. Data reflect an improvement in the filtration procedure in that the temperature of the fuel is measured directly over the fritted glass filter. Two methods of determining the mass of crystals frozen out of the fuel are available. The first, called Method 1, uses the value of the precipitate mass fraction and requires complete filtration of the fuel as well as accurate recovery of the filtrate and precipitate fractions. The second, Method 2, requires only a comparison of filtrate and initial fuel dye absorbances and densities. In Method 2, filtration can be stopped after a relatively small amount of filtrate is collected thus saving considerable test time. Results obtained via Method 2 will be compared with those obtained using Method 1.

In addition, we have measured weight fraction crystals vs. temperature for eight different hydrocarbon fuels.

2. HISTORICAL REVIEW

The Army was interested in the low temperature pumpability of fuels in the 1960's as shown by the work of Dimitroff et. al. [3]. It was found that plugging became a problem when about 3 percent of the fuel had crystallized. A liquid-solid separator was used for compositional analysis and saturated components were observed to freeze first. Through GC analysis, the occurrence of liquid entrapment within the crystalline matrix was deduced.

Noel investigated the DSC cooling curves of fuels and correlated the crystallization onset and peak temperatures with ASTM Cloud and Pour Points [4]. DSC analysis of petroleum products was continued by Giavarini and Pochetti [5]. Their data exhibit severe baseline drift, but nevertheless indicate the potential usefulness of DSC measurements in fuel oil evaluation. The linear relationship between the size of the melting endotherm, ΔH, and paraffin content was shown.

Faust later studied the melting behavior of paraffins using the Perkin Elmer DSC model 1B, which exhibited improved baseline control. He found cooling rate to effect the location of the exothermic peak temperature in the crystallization curves of paraffin waxes. This is caused by thermal resistance between the sample pan and the holder platform [6]. Difficulty in achieving thermal equilibrium is a primary problem of differential scanning calorimetry.

In the mid 1970's, with the threat of crude oil scarcity, the Navy saw the need for investigating alternate sources of jet fuel and their effect on product properties. Solash et. al. [7] determined the

compostions of shale-derived fuels and found them to be higher in n-alkane content and freeze point. These authors were able to correlate freezing point with C_{16} content of the fuel and also with the size of the aromatic molecules present.

Longwell and Grobman investigated likely future aircraft fuel properties and found the most probable changes to be increased aromatic content and increased distillation end point, the latter acting to raise the freezing and pour point temperatures [8]. Based on time-temperature data for typical commercial flights, they predict a resulting minimum fuel temperature of -43°C. To minimize the total cost of energy, manpower and materials necessary to adapt to these fuels, it was suggested that there must be a compromise between relaxed fuel specifications and limited redesign of the aircraft fuel system.

NASA has extensively investigated fuel trends, simulated flight conditions, and fuel circulation systems [9,10,11,12]. Using a wing tank simulator, the mass hold-up of the fuel was monitored under controlled conditions and correlated with its freezing properties. Beyond 10 percent hold-up, it was found that in addition to microcrystalline entrapment, large scale blockage of liquid containing no crystals occurs.

Friedman reported that more than half of the refineries surveyed claim that the maximum freezing point specification is the bottleneck in their jet fuel production. The majority of commercial flights can use higher freezing fuel (max. fp = -29°C), which would permit the use of lower grade crudes such as shale oil, tar sands and coal liquids.

Friedman recommends heating of the fuel tanks in flight as the most practical approach for the use of broader specification fuels in all weather conditions.

Wax Appearance and Pour Point do not necessarily correlate with fuel hold-up and pumpability. Interest has therefore focused more recently on the nature of the solid fraction of fuel and on methods to quickly and accurately characterize the fuel's low temperature flowability.

Moynihan has obtained melting and freezing points for a variety of fuels by DSC analysis [13] and has shown this technique to be a means of reliably and rapidly obtaining thermal data which more completely describe the nature of the freezing process compared to ASTM testing. A Perkin Elmer model DSC-2 was used with a heating rate of 5 °C/min through a temperature range of -65 to +25 °C. DSC methods can be used to determine the amount of frozen n-alkane in the fuel provided that the heats of formation of the various solid components which freeze out of the liquid are known and assumed to be equal and approximately constant throughout the temperature range studied. The accuracy of these calculations may be verified by comparison to weight percent solids results obtained by the filtration methods presented in this thesis.

Van Winkle and Affens isolated and characterized the precipitate fraction by GC analysis and found that it was composed of 70 to 80 percent entrapped liquid [14]. Moynihan et. al. later refined the separation technique with the use of tracer dyes which allowed the utilization of spectrophotometric methods for more accurately

determining the mass of crystals present in the partially frozen fuel [2]. This approach however foregoes the acquisition of compositional information.

3. EXPERIMENTAL PROCEDURE

3.1 Fuel Samples

Crystallization of eight fuels was studied. These were supplied by NASA - Lewis Research Center, Naval Research Laboratories, and the Naval Air Propulsion Center. Total normal paraffin content (C_9 through C_{19}) is in the range of 14 to 22 wt%. A description is given in Tables I-a and I-b. Further details may be found in NASA and NRL reports [9,15,16].

Prior to filtration the fuels were injected with two hydrocarbon soluble tracer dyes: 60 ppm CALCO Oil Blue G Liquid and 40 ppm CALCO Oil Orange R Liquid, both obtained from American Cynamid Co., Boundbrook, NJ. Fuels containing dye in this concentration are designated as "initial" fuels, while fuels containing no dye are referred to as "original" fuels.

3.2 Filtration

The fuel filtration apparatus consists of a liquid-solid separator constructed from 24 mm OD Pyrex glass tubing. The separator design is illustrated in Figure 1 and is similar to the one used at NRL [14]. The filter element is a medium porosity Pyrex fritted disc with a funnel tip extending below it.

The LSS is capped on the top and bottom with cup pieces joined to the body by rubber O-ring joints and clamps. The bottom piece collects the filtrate. Dry N_2 gas is regulated to 10 psig and is pre-cooled before it enters the filter chamber by first passing through a sufficient length of tygon tubing in a refrigerated methanol bath.

The bath is contained in a 4 liter unsilvered double walled dewar flask. Its temperature is maintained constant to ±0.1°C. The refrigerator coils (from a FTS Systems Inc. model LC-80 low temperature liquid cooler) continuously remove heat from the bath which is vigorously agitated. The temperature controller senses the bath temperature and regulates it to the set point via a 250 watt immersion heating rod.

Thermocouples are placed within the bath and inside the liquid-solid separator to monitor the temperature of the partially crystallized fuel immediately above the filter. Both thermocouples were calibrated against a NBS-certified Pt resistance thermometer.

Prior to filtration, the weight of the bottom glass piece together with a cork and supporting beaker are recorded. The bottom piece is then clamped onto the separator and tightened. The top glass piece is loosely clamped to the separator and 10 psig nitrogen is passed upwards through the filter. The LSS is then lowered into the bath to a depth where the upper N_2 connection is just covered by the bath.

The Method 1 filtration technique requires an accurate mass recovery of both the filtrate and precipitate fractions. The absorbance and density of each are subsequently measured. Method 2 requires only that the absorbance and density of the filtrate be known.

For Method 1, approximately 15 mℓ of initial fuel is placed into a small (30 mℓ) beaker and weighed to the nearest hundreth mg. The top piece of the LSS, which is attached to the thermocouple, is momentarily lifted and the fuel is carefully poured into the filter chamber. Spills are avoided by using the thermocouple stem as a

"drip-rod". The beaker is quickly reweighed to determine the amount of fuel left behind in the beaker.

Before pouring in the fuel, it is important to reduce the N_2 flow to prevent foam-up of the fuel on the filter. Sufficient pressure to hold the fuel above the filter is indicated by the rise of occasional small bubbles through the fuel. Due to the rapid increase in viscosity of the fuel as it is cooled, premature leakage through the filter is not a problem.

A digital millivoltmeter (Keithley model 177) was used for continual monitoring of the sample thermocouple during the crystallization and filtration steps.

If percent solids is to be determined by Method 2, a smaller quantity (5 to 7 mℓ) of fuel is adequate for the separation. Also, weighing of the fuel is unnecessary. A syringe is used to directly inject the fuel into the filter chamber.

The sample is allowed to crystallize at constant temperature for a minimum of 30 minutes. During this time it should be stirred at least twice. A glass spatula may be kept in the chamber for this purpose, but this introduces the risk of heat transfer to the fuel, and use of the thermocouple as a stirrer is preferred.

To commence filtration, the upper clamp is tightened and gas flow is diverted to the top of the filter. The voltage reading from the sample thermocouple is monitored throughout the filtration. The bath temperature is checked periodically. As filtration proceeds, the filter temperature will slowly increase as the fuel level drops. Some typical temperature profiles are shown in Figure 2. The fuel temperature is

approximately 2°C higher than that of the cooling bath due to poor thermal conduction to the bath along the filter disc and due to heat conduction down the thermocouple probe.

When a sufficient quantity of filtrate has been collected for the density and absorbance measurements required for Method 2, filtration may be suspended. For Method 1, the properties of the precipitate are needed and filtration must proceed until no more liquid can be collected.

Eventually, pockets of gas will form into channels in the precipitate. The small amount of remaining filtrate is held in place by the stiff solid. When channeling occurs, the gas selectively flows through the channels and does not effectively force the remaining liquid through the filter. The temperature increases more rapidly due to the convective heat brought by the increased gas flow. At some point it becomes necessary to interrupt the filtration so that the remaining fuel can be stirred in an attempt to break up the gas channels. Again, a glass spatula might be used, but in addition to the risk of heat transfer to the fuel, precipitates are "sticky" and their adherence to the spatula prevents them from being flattened down against the filter. It is recommended that the tip of the thermocouple be used to break up the crystals. The sudden small drops in filter temperature seen in Figure 2 indicate where filtration was temporarily disrupted so that gas channels in the precipitate could be broken up.

Upon resuming filtration, the gas pressure should be reduced to discourage channeling and allow gravity to draw down the last remaining liquid to the filter. When, despite these procedures, the

flow of filtrate is less than one drop per minute or when gas channeling results in vigorous bubble formation accompanied by a large temperature rise, filtration is suspended and nitrogen is rediverted to the bottom of the separator. Filtration usually requires between one and six hours depending on the fuel and the temperature. Some fuels are highly viscous at low temperatures and require the application of vacuum below the filter during part or all of the filtration.

The LSS is raised from the bath and dried off. The solid precipitate will immediately begin to melt but is held above the filter by N_2 pressure. The bottom glass piece containing filtrate is unclamped and quickly corked to prevent contamination from moisture condensation.

A preweighed 1 oz. sample bottle is placed under the filter and the gas is diverted to force the now-melted precipitate fraction through the filter disc. (This step is omitted in Method 2 and the precipitate is discarded.) Approximately 3-5 mℓ of normal pentane is used to rinse the upper walls of the filter chamber. The solvent is then pressured downward through the filter and collected with the precipitate. This rinsing step is repeated twice.

The mixture of pentane plus precipitate is next placed uncovered in a dark, cool spot so that the pentane may be allowed to evaporate for at least 12 hours before reweighing. Many of the fuels are light sensitive and must be stored in darkness to preserve their absorbance characteristics. Any residual $n\text{-}C_5H_{12}$ can be purged off with a low flow of dry N_2 above the liquid until the sample bottle attains a constant weight. The combined weight of the filtrate and precipitate

fractions is then recorded and percent recovery is calculated.

3.3 Density and Absorbance Measurements

Liquid densities were determined with Moore-Van Slyke specific gravity bottles. These were calibrated using distilled water at known temperatures. Care was taken to deliberately over-fill the bottles by a few drops to prevent air bubbles from being trapped in the neck piece. Excess fluid spurted out through the neck and was absorbed by a tissue which wrapped and held the top of the neck piece as it was inserted into the bottle.

Both Method 1 and Method 2 involve calculations which require a ratio of density values. It is necessary to measure the required densities for a given filtration at the same time so the ambient temperature is constant. The ratio value however is temperature independent and it is not a problem that room temperature may vary between measurements from different filtrations.

Absorbance data were obtained using a Perkin Elmer model 330 spectrophotometer. Silica sample cells with 1 cm thickness in the beam direction were used. Prior to each set of measurements, a background correction scan was run to correct for absorption differences between the sample cells. For this, each cell was filled about one half full with deionized water in order to simulate measurement conditions in which the cells are half filled with fuel.

After positioning a sample cell in the spectrophotometer, 10 to 15 minutes are needed for it to warm up and thermally equilibrate. As the fuel warms, it expands slightly and its absorption correspondingly decreases. It is therefore important that both the reference cell and

sample cell be at the same temperature.

Undyed (original) fuel is placed in the reference beam so that the absorption difference between the sample and the reference is due to the concentration of dye in the sample. Absorbance spectra were recorded in the range between 400 and 800 nm which spans the visible region. For calculations, four wavelengths were chosen which are predominantly attributable to either one or the other of the two dyes as shown in figure 3.

3.4 Melting Points

The ASTM melting point technique is such that the partially frozen fuel sample is allowed to warm at ambient temperature while being stirred. The temperature at which the crystals completely disappear is reported to the nearest 0.5°C. This dynamic procedure is likely to over-estimate the melting point.

To obtain a more reliable value, "equilibrium" melting points were measured by a static method in which approximately 20 mℓ of the partially frozen sample was kept in a temperature-regulated methanol bath and allowed to thermally equilibrate. The sample and stirrer dimensions approximated those specified by ASTM D 2386-67. As in the filtration experiments, the sample temperature was monitored using a calibrated thermocouple. It was positioned so that the tip was at the center of the sample and surrounded by the spirals of the stirrer. The temperature of the fuel was progressively increased by small increments (a few tenths of a °C or less) by increasing the bath temperature and continuously stirring. This was repeated until all of the crystals were melted.

Melting points obtained using the static method are in good agreement with DSC melting points [13,17] as shown in Table II. DSC melting point is the temperature corresponding to the point midway down the large endothermic peak observed upon slow heating (5-10°C/min) of the sample.

3.5 Pour Points

The formation of large wax crystals increases the tendency for plugging and a slow-cooled, maximum pour temperature should be identified. Pour points were therefore also measured by a static method in which the bath temperature was successively lowered in small increments (1°C or less) to allow the sample to thermally equilibrate.

The sample container complied with D97-66 specifications, being flat bottomed, air-jacketed and about 30 mm in diameter. Enough fuel was added to obtain a liquid level height of approximately 54 mm as also specified by the ASTM Pour Point test. A calibrated thermocouple was used to measure the sample temperature and placed so that the tip penetrated the surface center to a depth of about 5 mm.

When the fuel appeared sufficiently rigid, the container was raised from the bath and held horizontally for 5 seconds. If the fuel meniscus showed movement, the sample was cooled to slightly lower temperature and retested. If upon the first test, the fuel meniscus did not move, the container was allowed to warm to nearly melting temperature before placing again in the bath. It was then re-cooled to a temperature a few degrees higher than the initial temperature and retested. In this manner, the pour point result would not be affected

by any previous over-freezing of the fuel.

Even after considering cooling rate, the current technique of pour point measurement is such that the nature of the fuel is not considered. In some fuels, the bulk liquid may become viscous and congealed upon cooling. In this case, its stiffness is only partially due to a crystalline network structure. In other fuels, the bulk liquid retains high fluidity and the pour point is ultimately reached when a "skin" of more densely connected crystals on the liquid surface has attained sufficient rigidity to hold back the bulk. In this latter case, any movement of the thermocouple tip disrupts the rigid crystal skin and allows the less viscous bulk to break through when the sample is tipped. For such fuels, testing precision is low.

4. CALCULATION OF AMOUNT OF CRYSTALLINE SOLIDS

4.1 Mass Balance

The calculation of wt% solids is based upon the application of a dye mass balance to the filtrate and precipitate fraction and includes two key assumptions: first, that the dye molecules do not become a part of the frozen hydrocarbon crystalline matrix, but remain entirely in the liquid phase of the fuel; second, that absorbance is proportional to dye concentration in the range of concentrations encountered in this study. The development of these assumptions and subsequent calculations for Method 1 result in the following expression for wt% solids:

$$\%S = 100 \frac{m_p}{m_{in}} \left[1 - \frac{A_p}{A_f} \frac{\rho_f}{\rho_p} \right] \qquad (1)$$

where m_p and m_{in} are the masses of the recovered liquid precipitate and initial fuel; A_p and A_f are the absorbances of the precipitate and filtrate fractions; ρ_p and ρ_f are the corresponding densities at room temperature of the liquid precipitate and filtrate fractions [2].

If a dye mass balance is made between the the filtrate fraction and that of the initial fuel sample, a second expression for wt% solids can be derived as follows.

The mass of dye molecules in the initial fuel sample is split up into the filtrate fraction and the liquid portion of the precipitate fraction:

$$m_{dye} = \frac{C_{in}\, m_{in}}{\rho_{in}} = \frac{C_f\, m_f}{\rho_f} + \frac{C_\ell\, m_\ell}{\rho_\ell} \qquad (2)$$

C_{in}, C_f, and C_ℓ are the respective concentrations of dye tracer in the initial fuel, filtrate and entrapped liquid in the precipitate. ρ_{in}, ρ_f, and ρ_ℓ are the corresponding ambient temperature densities, while m_{in}, m_f, and m_ℓ are the corresponding masses. Since dye absorbance is proportional to concentration, Eq. 2 can be modified to read:

$$\frac{A_{in}\, m_{in}}{\rho_{in}} = \frac{A_f\, m_f}{\rho_f} + \frac{A_\ell\, m_\ell}{\rho_\ell} \qquad (3)$$

where A_{in}, A_f, and A_ℓ refer to the absorbance values for each of the fuel fractions. The entrapped liquid is identical in composition to the filtrate and therefore $A_\ell = A_f$; likewise, $\rho_\ell = \rho_f$.

Since the precipitate is made up of crystalline solid plus the entrapped liquid, while the initial fuel is comprised of precipitate plus filtrate, the mass of entrapped liquid can be expressed as:

$$m_\ell = m_{in} - m_f - m_s \qquad (4)$$

and Eq. 3 can now be rewritten as:

$$\frac{A_{in}\, m_{in}}{\rho_{in}} = \frac{A_f\, m_f}{\rho_f} + \frac{A_f(\, m_{in} - m_f - m_s\,)}{\rho_f} \qquad (5)$$

Rearranging, and solving for m_s:

$$m_s = m_{in} \left[1 - \frac{A_{in}\,\rho_f}{A_f\,\rho_{in}} \right] \qquad (6)$$

The percent of initial fuel which becomes solid at a given temperature is equal to 100 x (m_s/m_{in}) or:

$$\%S = 100 \left[1 - \frac{A_{in}\,\rho_f}{A_f\,\rho_{in}} \right] \qquad (7)$$

At the conditions studied, %S was typically less than 10%. Consequently, A_{in} was just slightly lower than the value of A_f. Experimental error is minimized by directly comparing A_f to A_{in}. This was done by placing the initial fuel in the reference beam and the filtrate in the sample beam. The difference in absorbance is ΔA where:

$$\Delta A = A_f - A_{in}$$

Eq. 7 can then be modified in either of two ways to introduce ΔA :

$$\%S = 100 \left[1 - \frac{(A_f - \Delta A)}{A_f} \frac{\rho_f}{\rho_{in}} \right] \qquad (8)$$

$$\%S = 100 \left[1 - \frac{A_{in}}{(A_{in} + \Delta A)} \frac{\rho_f}{\rho_{in}} \right] \qquad (9)$$

The experimental error associated with either of the above expressions is superior to that obtained by using Eq. 7 in which the

uncertainty of A_{in}/A_f is large compared to its magnitude.

The main advantage of using Eqs. 8 and 9 is that the mass, density and absorbance of the precipitate are not required. The filtration need only be conducted for a time sufficient to collect enough filtrate (about 3 mℓ) for density and absorbance measurements. Also, the time-consuming solvent rinse and evaporation procedure needed for complete recovery of the precipitate is eliminated. While Method 2 affords considerable saving of laboratory test time, it is associated with a slight increase in inherent experimental uncertainty. An accurate measurement of absorbance difference between two highly abosrbing solutions is necessary for accurate determination of the amount of solid.

4.2 Error Analysis

Inherent experimental error arises generally from a number of sources. If a variable, S, is a function of several parameters, K_i (i=1,2,...n), then the error in S, denoted as dS, can be defined by:

$$dS = \sum_{i=1}^{n} \left| \frac{\partial S}{\partial K_i} dK_i \right| \qquad (10)$$

The percentage, or relative error is 100 (dS/S) and the variable, S, is weight percent solid. For Method 1, this is given by Eq 1. An expression for dS/S can be obtained by differentiating Eq. 1 with respect to each of its parameters, and summing as shown by Eq. 10. Subsequently dividing by S results in:

$$\frac{dS}{S} = \frac{dm_p}{m_p} + \frac{dm_{in}}{m_{in}} + \left[\frac{1}{A_f\rho_p - A_p\rho_f}\right]\left[\rho_f\, dA_p + \frac{A_p\,\rho_f}{A_f}\, dA_f + A_p\, d\rho_f + A_p\,\rho_f\,\frac{d\rho_p}{\rho_p}\right] \qquad (11)$$

By noting the following simplifying assumptions: $\rho_f \approx \rho_p$, $d\rho_f \approx d\rho_p$, and both dm_p/m_p and $dm_{in}/m_{in} \ll 1$, it is convenient to reduce the above expression to:

$$\frac{dS}{S} = \frac{A_p}{A_f - A_p}\left[\frac{dA_p}{A_p} + \frac{dA_f}{A_f} + 2\,\frac{d\rho}{\rho}\right] \qquad (12)$$

Similar treatment of Eqs. 8 and 9 results in expressions describing relative error for Method 2:

$$\frac{dS}{S} = \frac{dA_f}{A_f} + \frac{d\Delta A}{\Delta A} + 2\,\frac{(A_f - \Delta A)}{\Delta A}\,\frac{d\rho}{\rho} \qquad (13)$$

$$\frac{dS}{S} = \left[\frac{A_{in}}{A_{in} + \Delta A}\right]\left[\frac{d\Delta A}{\Delta A} + \frac{dA_{in}}{A_{in}}\right] + 2\,\frac{A_{in}}{\Delta A}\,\frac{d\rho}{\rho} \qquad (14)$$

Values of dA_p, dA_f, dA_{in}, and $d\Delta A$ were estimated from the spectrophotometer model specifications which report absorbance error as ±0.002 for absorbance values between 0 and 0.5, and as ±0.004 for values between 0.5 and 1.

The parameter, ρ, is the average value of density of the two fractions being considered. The value of $d\rho$ was estimated, and depends on the number of measurements taken and the precision of the

measurements. Measurement precision is largely dependent on how reproducibly the specific gravity bottles can be filled. When two or more density results were obtained for one sample, the error was estimated to be one half the difference between the maximum and minimum values. A lower limit of $d_\rho = \pm 0.0001$ g/cm^3 was imposed on this estimate. For single measurement values, an error of ± 0.001 g/cm^3 was used. This latter default value is conservatively high since duplicate measurements typically did not vary by more than ± 0.0005 g/cm^3.

At low solid concentrations, the error for Method 2 is somewhat greater than that for Method 1 because the value of ΔA becomes small and consequently the term, $d\Delta A/\Delta A$ becomes large. This is more clearly illustrated in Table III which summarizes error estimates for LFP-3 measurements.

5. RESULTS

5.1 Beer's Law Experiment

The transmittance, T, of a material is defined as the ratio of transmitted beam intensity, I, to its incident intensity and is defined by the Lambert equation:

$$T = \frac{I}{I_o} = e^{-\beta x} \qquad (15)$$

where β is the absorption coefficient and is a function of wavelength. Specimen thickness is x. Beer defines β as equal to εC, where ε is the extinction coefficient, or absorption per unit concentration at a particular wavelength. C is the weight concentration of the absorbing species in g/cm^3.

Absorbance, A, is defined as -log T, so

$$A = \varepsilon C x / 2.3 \qquad (16)$$

Since x=1 cm for all measurements, absorbance is proportional to εC. Moynihan et. al. has shown that extinction coefficient is not dependent on hydrocarbon composition of the fuels and therefore the relative concentration of dye in the separated fractions can be obtained by measuring their relative absorbances [2].

To verify the accuracy and sensitivity of the spectrophotometer, known dilutions of varying dye concentrations were prepared and tested. The dilutions were made up of two constituents designated as "A" and "B". Constituent A was filtered, original NAPC-5.

Constituent B was initial NAPC-5, that is, NAPC-5 containing 100 ppm dye (60 ppm blue plus 40 ppm orange). The compositions of the test dilutions are given in Table IV-a.

The most dilute sample, #1, was used as the reference sample to which the other dye concentrations were compared. Absorbance difference, ΔA, was then measured for samples #2 through #6. Results at four wavelengths are plotted in Figure 4. As expected, absorbance is a linear function of dye concentration.

The accuracy of the slopes obtained in Figure 4 was verified to rule out the possibility of systematic machine error. This was accomplished by comparing the value of %S obtained from absorption measurements of samples #1-6 to that obtained by back-calculation using the known compositions of the samples.

In the former case, sample #1 was considered to be a pseudo initial fuel with samples #2-6 as the corresponding pseudo filtrates at various crystallization temperatures. A_{in}(pseudo) was obtained by measuring the absorbance of sample #1 vs. undyed NAPC-5. Equation 9 was then used to calculate percent solids associated with each of the filtrates. These data and calculations are summarized in Table IV-b.

Based on the known compositions of samples #1-6, a back-calculation of "actual" wt% solids can be derived as follows. Sample #1, the pseudo initial fuel, has a dye concentration, C_{in}, equal to (wt. fraction of constituent B) X (100 ppm) = 90.903 ppm from Table IV-a. Likewise, the dye concentrations of samples #2-6 are determined. By noting that concentration is proportional to absorbance, and $\rho_f = \rho_{in}$, equation (7) can be modified to:

$$\%S = 100 \left[1 - \frac{C_{in}}{C_f} \right] \qquad (17)$$

In Table V, the values of wt% S obtained from known dye concentrations of the dilutions are compared to values calculated from the absorbances of the samples. As expected, experimental error increases as absorbance difference between the filtrate and initial fuel (or ΔA) decreases. Even at 2 percent solids the error is small; however, and good agreement of results throughout the range of dilutions studied confirms consistent machine accuracy.

5.2 Fuel Absorbance Spectra

Figures 5 and 6 show absorbance spectra of the undyed fuels compared to distilled water in the reference beam. Typically these fuels exhibit little or no absorbance in the visible range but become quite strongly absorbing in the UV region. Of the eight fuels studied, four were distinctly higher absorbing in the visible range: Fuel #7, LFP-5, NAPC-2 and NAPC-5. The absorbance of each of these fuels is greater than 0.01 at 500 nm. Orange dye calculations require absorbance values at 480 and 508 nm; therefore, significant error may result from faulty interpretation of filtrate and precipitate absorbances which are presumed to be entirely attributable to the dye.

This problem is more clearly illustrated in Figure 7. Undyed NAPC-2 was partially frozen at -40°C and filtered. The absorbance spectra of each of the separated fractions vs. original fuel is shown. Original fuel was in the sample beam and the separated fractions were in the reference beam. The filtrate shows increased absorbance

relative to the original fuel while the precipitate fraction has lower absorbance. Clearly, the absorbing components of the the fuel generally do not freeze out initially and hence are concentrated in the filtrate.

This compositional effect makes it necessary to neglect orange dye measurements for certain fuels. Such fuels may be selected by a maximum absorbance criteria; it is suggested that 0.01 at 500 nm be used. Fuels having a yellow color generally fall into this category.

5.3 Fuel Filtration Experiments

Tables VI through XVIII summarize Method 1 and Method 2 filtration results for each of the fuels. For Method 1, the mass of each fraction is included. Table XIX additionally summarizes mass percent precipitate (%P), mass percent recovery, and error estimates for the Method 1 filtration experiments.

$$\%P = 100\ m_p\ /\ m_{in}$$

$$\%recovery = 100\ (m_f + m_p)\ /\ m_{in}$$

Weight percent solid was calculated from absorbance measurements at four wavelengths corresponding to prominent maxima of the spectra. The agreement between wt% solid calculated from blue dye measurements (650 and 601 nm) and from orange dye measurements (508 and 480 nm) was poor for those fuels which, with no dye, exhibited strong absorbance in the near UV range. These include Fuel #7, LFP-5, NAPC-2 and NAPC-5, all having greater than 0.01

absorbance at 500 nm. The reported value of solids content was consequently the average of either two or four calculations depending on whether the orange dye measurements were rejected or accepted per the defined absorbance criterion.

Figures 8 through 15 show wt% solid plotted as a function of average fuel filtration temperature as recorded by the thermocouple directly over the glass frit. The temperature plotted at zero percent solid corresponds to the equilibrium melting point of the fuel.

Calculations of percent error obtained with Method 1 show the results to be reliable within a range varying from ±0.1 to ±0.5 weight percent solid depending primarily on the amount of solids measured. Comparable results via Method 2 are reliable within a error margin of ±0.3 to ±0.5 weight percent solid. The lesser error associated with Method 1 is observable at low solid concentrations as expected.

5.4 Effect of Pour Point Depressant

Fuel #7 and LFP-5 are identical except for the addition of 0.1% pour additive to the former. Mechanisms of pour point depressants have been postulated but not yet substantiated. It is generally agreed that the first components to freeze out are the normal alkanes, primarily C_{14} - C_{16}, which incur little thermodynamic resistance to crystal nucleation because of their low crystal-liquid interfacial tension [18]. Crystal growth is accompanied by an inclination to chain segment alignment; eventually, intersecting segments comprise an open matrix structure within which liquid becomes trapped. It is speculated that pour additives are adsorbed onto the surfaces of the solid where they inhibit further chain alignment thus preventing the formation of a

connected solid matrix.

It has been observed that such additives do not change the Cloud Point of the fuel. Note also that the melting points of LFP-5 and Fuel #7 are equal within experimental error, which suggests that the crystallization process of the n-alkanes is unaffected. An inhibition of crystal aggregation can likely be inferred. The distribution of wax content is important, since the additives are less effective if the n-alkanes are within a narrow freezing range [19,20].

ASTM Pour points are measured at a standardized high rate of cooling and are defined as the temperature 5°F above that which the meniscus does not move when the sample is held in a horizontal position. This procedure may not be adequate for predicting the fuel's characteristics under conditions of slow cooling such as experienced in an aircraft wing tank. Cooling rate has a critical effect on the wax structure with large crystals and a corresponding gel-like appearance resulting from a slow cooling rate at temperatures higher than the ASTM Pour Point.

Crystal growth begins near the Cloud Point and initially the rate is high. As temperature decreases, the bulk liquid becomes more viscous which retards the rate of crystal growth. (Additives used to depress the pour point do not prevent the viscosity increase of uncrystallized components.) Fuels with similar cloud and pour points may therefore have different flow characteristics due to their liquid properties [21,22].

Table XX lists fuel pour points obtained with a cooling rate of approximately $\frac{1}{4}$°C per minute. The wt% solid corresponding to each

of these pour points is included. Addition of 0.1% pour additive to LFP-5 decreases its pour point by 16°C.

The resistance to nucleation has been correlated with a parameter called reduced undercooling, ΔT_r, which is defined as equal to $(T_m - T)/T_m$. It may be reasoned that, at equivalent differences in temperature from their melting temperatures, the fuels will exhibit similar tendencies to crystallize. On this basis, the individual natures of the precipitate fractions can be more easilly compared.

Figure 16 shows the relation between solids concentration in the precipitate at the completion of the filtration vs. °C below the melting point for five fuels. (On an absolute scale, their melting temperatures are similar and therefore $T_m - T$ is used instead of ΔT_r.)

It can be seen that Fuel #7 has lower liquid concentration in the precipitate fraction than LFP-5 at a given value of $T_m - T$. This is an indication that the crystalline structure of the former is more loosely connected and therefore not as efficient at trapping liquid. This difference is a maximum at 17°C below their melting points where the Fuel #7 precipitate contains 40% solids compared to 12% solids in the LFP-5 precipitate.

The pour point of Fuel #7 (-52°C) occurs at 23°C below its melting temperature while the pour point of LFP-5 (-36°C) occurs at only 7°C below its melting point. At their respective pour point temperatures, the LFP-5 precipitate contains 19% solid crystals compared to 33% crystals in the Fuel #7 precipitate. Also, at their pour points, LFP-5 and Fuel #7 contain 3.4% and 7.7% solid as mass percentage of total fuel. Despite the higher viscosity of the bulk

liquid at -52°C compared to -36°C, the pour additive in Fuel #7 allows it to retain fluidity with higher crystal content.

The apparent maxima seen in the curves of Figure 16 can be explained by the effect of bulk liquid viscosity. Initially, the concentration of solid in the precipitate is low. It can be inferred that, at temperatures close to the fuel's melting point, the crystalline network is thin-walled and "spidery" but nevertheless well inter-connected and consequently efficient at containing a large amount of liquid within its structure.

At lower temperatures, more crystals are formed. The existing matrix supplies nucleation sites for further growth which results in the walls of the network structure becoming thicker. Thus the relative liquid content of the precipitate decreases. At very low temperatures, however, the increased viscosity of the remaining bulk liquid becomes significant. Diffusion is inhibited and the additional crystal nucleii are scattered and relatively immobile. Even so, the liquid has attained enough rigidity so that it is easilly held back from the filter by the initially developed solid matrix. Thus, the precipitate retains a large amount of liquid.

6. DISCUSSION AND CONCLUSIONS

Method 1 provides a means of accurately determining the amount of crystalline solid in a partially frozen fuel. Completion of the weighing, filtration and evaporation steps usually takes 15 to 18 hours. Method 2 enables similar results to be obtained in only a few hours. While Method 2 introduces some experimental inaccuracy, comparison of results obtained by the two methods, as shown in Figures 8-12, indicate acceptable agreement and therefore data obtained by Method 2 alone are considered satisfactory.

Before using orange dye absorbance measurements, it is first necessary to screen the original fuel for its natural absorbance at the shorter wavelengths. Fuels having an absorbance greater than 0.01 at 500 nm risk having unequal absorbance characteristics in their precipitate and filtrate fractions thus introducing large error in the filtration calculations. In the absence of these complications, however, data obtained from the orange and blue dyes give the same results. The orange dye was originally introduced to obtain absorption data over a wide range of wavelengths and the verify that, between the initial fuel and its separated fractions, there is no compositional dependence of the extinction coefficient within this range [2]. Consequently, it may be concluded that only the blue dye is really necessary.

The fuel separation technique is useful in verifying the accuracy of solids concentration determined by DSC measurements. Equilibrium melting points show a close correspondence to DSC melting points. ASTM testing alone provides only limited information on the low

temperature properties of a fuel and the prescribed quick-cooling conditions discourage repeatability and do not approximate the slow cooling conditions which would likely be encountered by fuels in aircraft storage compartments.

The standardization of a useful dynamic, or flow test would be a complex undertaking. The equilibrium pour point technique is a simpler approach to more realistically evaluating a fuel's low temperature behavior.

REFERENCES CITED

1. "Petroleum Products and Lubricants, Parts 23-(I), 24-(II), 25-(III)", Annual Book of ASTM Standards, American Society for Testing and Materials, Philadelphia.

2. C. T. Moynihan, R. Mossadegh, and A. J. Bruce, "Determination of the Mass Fraction of Crystals in Partly Frozen Hydrocarbon Fuels", Fuel, 63, 378-384 (1983).

3. E. Dimitroff, J. T. Gray, Jr., N. T. Meckel and R. D. Quillian, Jr., Seventh World Petroleum Congress, Vol. VIII, Part 2, Elsevier, NY, p.141, 1967.

4. F. Noel and L. W. Corbett, J. Inst. Pet., 56, 261 (1970).

5. C. Giavarini and F. Pochetti, J. Therm. Anal., 5, 83, (1973).

6. H. R. Faust, 'The Thermal Analysis of Waxes and Petroleum', presented at the Seventh North American Thermal Analysis Society Conf., St. Louis, Sept. 25-28, 1977.

7. J. Solash, R. N. Hazlett, J. M. Hall, and C. J. Nowack, "Relation Between Fuel Properties and Chemical Composition. 1. Jet Fuels from Coal, Oil Shale, and Tar Sands", Fuel, 57, 521-528 (1978).

8. J. P. Longwell and J. Grobman, J. of Engr. for Power, 101, 155 (1979).

9. F. J. Stockemer, "Experimental Study of Low Temperature Behavior of Aviation Turbine Fuels in a Wing Tank Model", Report No. CR-159615, N.A.S.A.-Lewis Research Center, Cleveland, OH, 1979.

10. R. Friedman, "High-Freezing-Point Fuels Used for Aviation Turbine Engines", Manuscript No. 79-GT-141, presented at the Gas Turbine Conference and Exhibit and Solar Energy Conference, San Diego, CA, March 12-15, 1979.

11. R. Friedman, "Recent Trends in Aviation Turbine Fuel Properties", N.A.S.A. Technical Paper 2056, October, 1982.

12. R. Friedman and F. J. Stockemer, "Heating Experiments for Flowability Improvement of Near-Freezing Aviation Fuel", J. of Aircraft, 21, No. 4, 250-255 (1984).

13. C. T. Moynihan, M. R. Shahriari and T. Bardakei, "Thermal Analysis of Melting and Freezing of Jet and Diesel Fuels", Thermochimica Acta, 52, 131-141 (1982).

14. T. L. Van Winkle and W. A. Affens, "Jet Fuel Freezing Point

and Composition", presented at the 1982 Summer National AIChE Meeting, Cleveland, OH, Aug.29 - Sept.1, 1982.

15. J. Solash, R. N. Hazlett, J. C. Burnett, E. Beal and J. M. Hall, Paper #16 from ACS Symposium Series No. 163; Oil Shale, Tar Sands and Related Materials, H. C. Stauffer, ed. (1981).

16. W. A. Affens, J. M. Hall, E. Beal, R. N. Hazlett and J. T. Leonard, Paper #17 from .....ibid.

17. C. T. Moynihan et. al., "Thermal Properties of Fuels", Boeing Military Airplane Co. Final Technical Report, June 17, 1985.

18. D. Turnbull and F. Spaepen, "Crystal Nucleation and the Crystal Melt Interfacial Tension in Linear Hydrocarbons", J. of Polymer Sci., Polymer Symposium 63, 237-243 (1978).

19. S. R. Lebedev, R. M. Berezina and Ya. B. Chertkov, "Pour-Depressant Additives for Diesel Fuels", Chem. Tech. Fuel Oils, 11, No. 9-10, 1975.

20. J. L. Tiedji, Sixth World Petroleum Congress, Section VI, Paper 1, p.293, June 26, 1963.

21. F. J. Pass, C. Csoklich and K. Wastl, "Solid Paraffins and Low Temperature Characteristics of Petroleum Products", Seventh World Petroleum Congress, Vol. VIII, Part 2, Elsevier, NY, 129-39 (1967).

22. H. F. Deen, A. M. Kaestner and C. M. Stendahl, "Additives to Improve Quality and Low Temperature Handling of Middle Distillate and Residual Fuels", Seventh World Petroleum Congress, Vol. VIII, Part 2, Elsevier, NY, 41-56 (1967).

Table I-a

Fuels Used in Filtration Study

Fuel I.D.	Description / Source
LFP-3	paraffinic diesel ,NASA - LRC
LFP-5	paraffinic distillate ,NASA - LRC
Fuel #7	LFP-5 plus 0.1% pour point depressant
LFPA-3	aviation turbine blend ,NASA - LRC
Shale II JP-5	Paraho shale-derived kerosene jet fuel - NRL
NAPC-2 *	modified JP-5; Suntech, Marcus Hook, PA
NAPC-3 *	" " " "
NAPC-5 *	low aromatic JP-5

* Naval Air Propulsion Center

Table I-b

Select Reported Fuel Properties

Fuel ID:	LFP-3	LFP-5	Fuel #7	Shale II JP-5
Distillation, °C				
IBP	177	174	170	150
10%	219	214	214	177
90%	297	281	279	245
ASTM mp, °C	-16.5	-28.2	-27.6	-48.6
ASTM fp, °C	-19.3	-30.5	-32.2	-49.7
n-Alkane wt.%				
C_8	.01	.08		
C_9	.24	.22		.14
C_{10}	.57	.56		4.20
C_{11}	1.06	1.07		7.23
C_{12}	1.64	1.91		6.08
C_{13}	2.36	2.47		3.30
C_{14}	2.76	2.31		.93
C_{15}	2.93	2.42		.28
C_{16}	2.37	1.51		.06
C_{17}	1.95	.82		.01
C_{18}	1.32	.38		
C_{19}	.77	.13		
C_{20}	.31	.06		
Total	18.4	13.9		22.2

Table I-b (continued)

Select Reported Fuel Properties

Fuel ID:	NAPC-2	NAPC-3	NAPC-5
Distillation, °C			
IBP	168	171	181
10%	227	192	199
90%	272	261	243
ASTM fp, °C	-24	-34	-50
n-Alkane wt.%			
C_8	.09	.07	.05
C_9	.19	.20	.30
C_{10}	.31	.86	1.80
C_{11}	.60	4.07	3.99
C_{12}	.91	3.89	3.87
C_{13}	1.80	3.35	3.40
C_{14}	4.46	2.70	1.66
C_{15}	5.42	2.35	.77
C_{16}	2.85	1.39	.17
C_{17}	.64	.42	.03
Total	17.3	19.2	16.0

Table II

Equilibrium and DSC Fuel Melting Points

Fuel ID	DSC mp., °C	Equilibrium mp., °C
LFP-3	-16.8	-17.6
LFP-5	-28.9	-28.7
Fuel #7	-28.7	-27.4
LFPA-3		-44.4
Shale II JP-5	-50	-49.8
NAPC-2	-25.9	-26.1
NAPC-3	-36.3	-35.7
NAPC-5	-50	-50.0

Table III
LFP-3 Error Analysis

Data is the average of results at 4 wavelengths.
S = wt% solid
dS = absolute error in S
100(dS/S) = relative error as percent of S

Data for Method 1 Filtrations
Percent error calculated from Eq. 12

A_f	0.764	0.772	0.776	0.801	0.822
dA_f	0.004	0.004	0.004	0.004	0.004
A_p	0.587	0.518	0.535	0.595	0.620
dA_p	0.003	0.003	0.003	0.003	0.003
ρ	0.815	0.814	0.814	0.816	0.820
$d\rho$	0.001	0.001	0.001	0.001	0.001
100(dS/S)	4.2	2.7	3.0	3.6	3.7
S	2.87	4.97	4.72	7.63	9.32
dS	0.12	0.13	0.14	0.28	0.35

Data for Method 2 Filtrations
Percent Error calculated from Eq. 13

ΔA	0.039	0.039	0.061	0.082	0.107
$d\Delta A$	0.002	0.002	0.002	0.002	0.002
A_f	0.775	0.775	0.802	0.821	0.850
dA_f	0.004	0.004	0.004	0.004	0.004
ρ	0.819	0.820	0.821	0.824	0.820
$d\rho$	0.0006	0.0006	0.001	0.001	0.001
100(dS/S)	8.4	8.4	6.7	5.1	4.0
S	4.66	4.52	7.17	9.26	11.97
dS	0.39	0.38	0.48	0.47	0.48

Table IV-a

Sample Compositions for Beer's Law Experiment

Sample No.	Wt.% Component B	Relative Dye Concentration*
1	90.903	1.000
2	92.734	1.020
3	94.761	1.042
4	96.549	1.062
5	98.174	1.080
6	100.000	1.100

* (sample ppm) ÷ (sample #1 ppm)

Table IV-b

Spectrophotometric Determination of Wt.% Solids

for Beer's Law Experiment

Wavelength, nm	650	601	508	480
Sample #1, A_{in}	.663	.585	.630	.714
Sample #2, ΔA	.013	.011	.012	.013
%S	1.9	1.8	1.9	1.8
Sample #3, ΔA	.029	.025	.025	.029
%S	4.1	4.0	3.8	3.9
Sample #4, ΔA	.042	.036	.038	.044
%S	6.0	5.8	5.6	5.7
Sample #5, ΔA	.054	.047	.049	.056
%S	7.5	7.4	7.1	7.3
Sample #6, ΔA	.068	.059	.062	.071
%S	9.2	9.2	9.0	9.0

Table V

Verification of Spectrophotometer Performance

Using Beer's Law Experiment

Sample No.	"actual" %S (eqn. 17)	Measured %S (from eqn. 9)			
		Blue Dye [1]	% Error	Orange Dye [2]	% Error
2	1.97	1.85	-6.1	1.85	-6.1
3	4.07	4.05	-0.5	3.85	-5.4
4	5.85	5.9	+0.9	5.65	-3.4
5	7.41	7.45	-0.5	7.2	-2.8
6	9.10	9.2	+1.1	9.0	-1.1

(1) Avg. of 2 results for λ=650 and 601 nm

(2) Avg. of 2 results for λ=508 and 480 nm

Table VI

Method 1 Filtration and Dye Absorbance Data for Fuel #7

	Initial Fuel	Filtrate	Precipitate	Wt.% Solids
Average Filtration Temp. = -33.9°C Solids = 1.7 wt% (Blue Dye Avg.)				
mass, g	39.324	36.506	2.719	
density, g/mℓ		.825	.806	
abs. at 650 nm		.732	.539	1.71
abs. at 601 nm		.644	.484	1.60
abs. at 508 nm		.671	.484	1.82
abs. at 480 nm				
Average Filtration Temp. = -39.2°C Solids = 3.5 wt% (Blue Dye Avg.)				
mass, g	25.131	22.305	2.764	
density, g/mℓ		.825	.802	
abs. at 650 nm		.749	.490	3.61
abs. at 601 nm		.660	.442	3.43
abs. at 508 nm		.683	.430	3.89
abs. at 480 nm				
Average Filtration Temp. = -39.2°C Solids = 3.8 wt% (Blue Dye Avg.)				
mass, g	25.282	22.275	2.946	
density, g/mℓ		.825	.803	
abs. at 650 nm		.745	.486	3.86
abs. at 601 nm		.658	.436	3.73
abs. at 508 nm		.681	.423	4.23
abs. at 480 nm				
Average Filtration Temp. = -44.1°C Solids = 5.5 wt% (Blue Dye Avg.)				
mass, g	12.144	10.508	1.614	
density, g/mℓ		.828	.799	
abs. at 650 nm		.763	.430	5.54
abs. at 601 nm		.674	.384	5.46
abs. at 508 nm		.705	.367	6.14
abs. at 480 nm				

Table VI(continued)

Method 1 Filtration and Dye Absorbance Data for Fuel #7

	Initial Fuel	Filtrate	Precipitate	Wt.% Solids
Average Filtration Temp. = -44.1°C Solids = 5.6 wt% (Blue Dye Avg.)				
mass, g	12.114	10.474	1.627	
density, g/mℓ		.825	.798	
abs. at 650 nm		.762	.431	5.58
abs. at 601 nm		.675	.384	5.54
abs. at 508 nm		.704	.362	6.30
abs. at 480 nm				
Average Filtration Temp. = -49.1°C Solids = 6.7 wt% (Blue Dye Avg.)				
mass, g	11.970	9.779	2.169	
density, g/mℓ		.828	.801	
abs. at 650 nm		.776	.468	6.84
abs. at 601 nm		.685	.422	6.60
abs. at 508 nm		.715	.412	7.34
abs. at 480 nm				
Average Filtration Temp. = -49.3°C Solids = 6.7 wt% (Blue Dye Avg.)				
mass, g	12.113	9.854	2.227	
density, g/mℓ		.827	.800	
abs. at 650 nm		.777	.474	6.82
abs. at 601 nm		.686	.426	6.61
abs. at 508 nm		.718	.419	7.32
abs. at 480 nm				
Average Filtration Temp. = -54.2°C Solids = 8.2 wt% (Blue Dye Avg.)				
mass, g	12.498	8.587	3.865	
density, g/mℓ		.828	.809	
abs. at 650 nm		.797	.572	8.24
abs. at 601 nm		.701	.507	8.06
abs. at 508 nm		.728	.498	9.31
abs. at 480 nm				

Table VII

Method 2 Filtration and Dye Absorbance Data for Fuel #7

	Initial Fuel	Filtrate	ΔA	Wt.% Solids
Average Filtration Temp. = -34.5°C Solids = 1.6 wt% (Blue Dye Avg.)				
density, g/mℓ	.823	.824		
abs. at 650 nm		.732	.014	1.82
abs. at 601 nm		.648	.010	1.45
abs. at 508 nm		.678	.010	1.38
abs. at 480 nm				
Average Filtration Temp. = -39.4°C Solids = 3.5 wt% (Blue Dye Avg.)				
density, g/mℓ	.823	.825		
abs. at 650 nm		.748	.030	3.78
abs. at 601 nm		.661	.023	3.25
abs. at 508 nm		.696	.028	3.80
abs. at 480 nm				
Average Filtration Temp. = -39.4°C Solids = 4.0 wt% (Blue Dye Avg.)				
density, g/mℓ	.823	.826		
abs. at 650 nm		.752	.034	4.23
abs. at 601 nm		.665	.027	3.77
abs. at 508 nm		.699	.031	4.14
abs. at 480 nm				
Average Filtration Temp. = -44.4°C Solids = 5.2 wt% (Blue Dye Avg.)				
density, g/mℓ	.823	.826		
abs. at 650 nm		.762	.044	5.40
abs. at 601 nm		.674	.036	4.96
abs. at 508 nm		.712	.044	5.80
abs. at 480 nm				

Table VII (continued)

Method 2 Filtration and Dye Absorbance Data for Fuel #7

	Initial Fuel	Filtrate	ΔA	Wt.% Solids
Average Filtration Temp. = -44.4°C Solids = 5.9 wt% (Blue Dye Avg.)				
density, g/mℓ	.823	.826		
abs. at 650 nm		.768	.050	6.24
abs. at 601 nm		.678	.040	5.62
abs. at 508 nm		.714	.046	6.17
abs. at 480 nm				
Average Filtration Temp. = -49.9°C Solids = 7.0 wt% (Blue Dye Avg.)				
density, g/mℓ	.823	.827		
abs. at 650 nm		.778	.060	7.27
abs. at 601 nm		.687	.049	6.69
abs. at 508 nm		.725	.057	7.42
abs. at 480 nm				
Average Filtration Temp. = -49.7°C Solids = 7.3 wt% (Blue Dye Avg.)				
density, g/mℓ	.823	.828		
abs. at 650 nm		.781	.063	7.56
abs. at 601 nm		.690	.052	7.02
abs. at 508 nm		.729	.061	7.86
abs. at 480 nm				
Average Filtration Temp. = -54.6°C Solids = 8.6 wt% (Blue Dye Avg.)				
density, g/mℓ	.823	.828		
abs. at 650 nm		.792	.074	8.80
abs. at 601 nm		.700	.062	8.31
abs. at 508 nm		.739	.071	9.07
abs. at 480 nm				

Table VIII

Method 1 Filtration and Dye Absorbance Data for Shale II JP-5

	Initial Fuel	Filtrate	Precipitate	Wt.% Solids
Average Filtration Temp. = -52.6°C Solids = 2.9 wt% (Avg. of Both Dyes)				
mass, g	11.941	10.779	1.134	
density, g/mℓ		.799	.783	
abs. at 650 nm		.751	.512	2.90
abs. at 601 nm		.664	.454	2.88
abs. at 508 nm		.671	.456	2.92
abs. at 480 nm		.758	.511	2.98
Average Filtration Temp. = -52.6°C Solids = 3.1 wt% (Avg. of Both Dyes)				
mass, g	12.506	11.142	1.314	
density, g/mℓ		.799	.783	
abs. at 650 nm		.755	.521	3.12
abs. at 601 nm		.667	.462	3.09
abs. at 508 nm		.675	.464	3.15
abs. at 480 nm		.763	.521	3.20
Average Filtration Temp. = -52.4°C Solids = 2.8 wt% (Avg. of Both Dyes)				
mass, g	12.249	11.003	1.195	
density, g/mℓ		.800	.783	
abs. at 650 nm		.756	.532	2.76
abs. at 601 nm		.668	.473	2.71
abs. at 508 nm		.678	.473	2.82
abs. at 480 nm		.766	.531	2.86

Table VIII (continued)

Method 1 Filtration and Dye Absorbance Data for Shale II JP-5

	Initial Fuel	Filtrate	Precipitate	Wt.% Solids
Average Filtration Temp. = -52.7°C Solids = 2.9 wt% (Avg. of Both Dyes)				
mass, g	12.186	10.893	1.224	
density, g/mℓ		.800	.783	
abs. at 650 nm		.756	.532	2.84
abs. at 601 nm		.668	.473	2.80
abs. at 508 nm		.678	.473	2.90
abs. at 480 nm		.766	.533	2.92
Average Filtration Temp. = -54.4°C Solids = 4.0 wt% (Avg. of Both Dyes)				
mass, g	12.376	10.663	1.610	
density, g/mℓ		.802	.781	
abs. at 650 nm		.764	.523	3.91
abs. at 601 nm		.675	.464	3.87
abs. at 508 nm		.681	.463	3.97
abs. at 480 nm		.770	.519	4.05
Average Filtration Temp. = -54.3°C Solids = 4.4 wt% (Avg. of Both Dyes)				
mass, g	12.218	10.456	1.64	
density, g/mℓ		.8009	.782	
abs. at 650 nm		.777	.520	4.35
abs. at 601 nm		.683	.460	4.29
abs. at 508 nm		.691	.459	4.42
abs. at 480 nm		.780	.514	4.50

Table VIII (continued)

Method 1 Filtration and Dye Absorbance Data for Shale II JP-5

	Initial Fuel	Filtrate	Precipitate	Wt.% Solids
Average Filtration Temp. = -56.3°C Solids = 6.1 wt% (Avg. of Both Dyes)				
mass, g	11.925	9.556	2.310	
density, g/mℓ		.801	.783	
abs. at 650 nm		.785	.531	6.00
abs. at 601 nm		.692	.470	5.94
abs. at 508 nm		.698	.471	6.03
abs. at 480 nm		.790	.526	6.21
Average Filtration Temp. = -57.1°C Solids = 5.6 wt% (Avg. of Both Dyes)				
mass, g	12.124	9.362	2.628	
density, g/mℓ		.801	.787	
abs. at 650 nm		.784	.574	5.58
abs. at 601 nm		.690	.507	5.52
abs. at 508 nm		.699	.508	5.70
abs. at 480 nm		.791	.573	5.75
Average Filtration Temp. = -56.8°C Solids = 5.1 wt% (Avg. of Both Dyes)				
mass, g	8.329	6.091	2.042	
density, g/mℓ		.8005	.7852	
abs. at 650 nm		.796	.625	5.01
abs. at 601 nm		.701	.551	4.99
abs. at 508 nm		.712	.555	5.16
abs. at 480 nm		.807	.626	5.25

Table IX

Method 2 Filtration and Dye Absorbance Data for Shale II JP-5

	Initial Fuel	Filtrate	ΔA	Wt.% Solids
Average Filtration Temp. = -53.0°C Solids = 2.5 wt% (Avg. of Both Dyes)				
density, g/mℓ	.800	.802		
abs. at 650 nm		.749	.0235	2.94
abs. at 601 nm		.672	.0185	2.56
abs. at 508 nm		.689	.0165	2.20
abs. at 480 nm		.777	.019	2.25
Average Filtration Temp. = -53.1°C Solids = 2.6 wt% (Avg. of Both Dyes)				
density, g/mℓ	.7963	.798		
abs. at 650 nm		.759	.0225	2.76
abs. at 601 nm		.668	.0185	2.57
abs. at 508 nm		.675	.0175	2.39
abs. at 480 nm		.763		
Average Filtration Temp. = -53.1°C Solids = 2.4 wt% (Avg. of Both Dyes)				
density, g/mℓ	.7963	.799		
abs. at 650 nm		.757	.0225	2.68
abs. at 601 nm		.668	.018	2.40
abs. at 508 nm		.676	.016	2.08
abs. at 480 nm		.763		

Table IX (continued)

Method 2 Filtration and Dye Absorbance Data for Shale II JP-5

	Initial Fuel	Filtrate	ΔA	Wt.% Solids
Average Filtration Temp. = -55.1°C Solids = 4.1 wt% (Avg. of Both Dyes)				
density, g/mℓ	.7963	.799		
abs. at 650 nm		.772	.036	4.35
abs. at 601 nm		.680	.030	4.10
abs. at 508 nm		.688	.0295	3.98
abs. at 480 nm		.778		
Average Filtration Temp. = -55.1°C Solids = 4.2 wt% (Avg. of Both Dyes)				
density, g/mℓ	.7963	.800		
abs. at 650 nm		.772	.037	4.35
abs. at 601 nm		.681	.032	4.25
abs. at 508 nm		.689	.0315	4.13
abs. at 480 nm		.779		
Average Filtration Temp. = -55.2°C Solids = 4.4 wt% (Avg. of Both Dyes)				
density, g/mℓ	.800	.803		
abs. at 650 nm		.762	.037	4.50
abs. at 601 nm		.682	.0315	4.26
abs. at 508 nm		.698	.032	4.23
abs. at 480 nm		.787	.0375	4.41

Table IX (continued)

Method 2 Filtration and Dye Absorbance Data for Shale II JP-5

	Initial Fuel	Filtrate	ΔA	Wt.% Solids
Average Filtration Temp. = -56.9°C Solids = 5.7 wt% (Avg. of Both Dyes)				
density, g/mℓ	.800	.804		
abs. at 650 nm		.775	.0495	5.90
abs. at 601 nm		.694	.0415	5.50
abs. at 508 nm		.716	.044	5.66
abs. at 480 nm		.808	.0515	5.89
Average Filtration Temp. = -57.4°C Solids = 6.0 wt% (Avg. of Both Dyes)				
density, g/mℓ	.7963	.800		
abs. at 650 nm		.784	.053	6.28
abs. at 601 nm		.692	.0455	6.09
abs. at 508 nm		.702	.0445	5.85
abs. at 480 nm		.794	.048	5.56
Average Filtration Temp. = -57.6°C Solids = 6.5 wt% (Avg. of Both Dyes)				
density, g/mℓ	.7963	.801		
abs. at 650 nm		.786	.057	6.74
abs. at 601 nm		.694	.049	6.54
abs. at 508 nm		.703	.0485	6.38
abs. at 480 nm		.796	.0535	6.20

Table X

Method 1 Filtration and Dye Absorbance Data for LFP-3

	Initial Fuel	Filtrate	Precipitate	Wt.% Solids
Average Filtration Temp. = -23.1°C Solids = 2.9 wt% (Avg. of Both Dyes)				
mass, g	25.685	22.306	3.314	
density, g/mℓ		.820	.810	
abs. at 650 nm		.803	.619	2.84
abs. at 601 nm		.707	.544	2.86
abs. at 508 nm		.728	.558	2.90
abs. at 480 nm		.817	.628	2.87
Average Filtration Temp. = -27.2°C Solids = 5.0 wt% (Avg. of Both Dyes)				
mass, g	12.837	10.779	2.018	
density, g/mℓ		.822	.805	
abs. at 650 nm		.811	.546	4.93
abs. at 601 nm		.714	.482	4.90
abs. at 508 nm		.737	.492	5.03
abs. at 480 nm		.827	.552	5.03
Average Filtration Temp. = -27.7°C Solids = 4.7 wt% (Avg. of Both Dyes)				
mass, g	12.288	10.303	1.939	
density, g/mℓ		.822	.807	
abs. at 650 nm		.815	.564	4.67
abs. at 601 nm		.719	.497	4.68
abs. at 508 nm		.740	.507	4.78
abs. at 480 nm		.830	.571	4.74

Table X (continued)

Method 1 Filtration and Dye Absorbance Data for LFP-3

	Initial Fuel	Filtrate	Precipitate	Wt.% Solids
Average Filtration Temp. = -33.2°C Solids = 7.6 wt% (Avg. of Both Dyes)				
mass, g	12.509	8.595	3.900	
density, g/mℓ		.823	.809	
abs. at 650 nm		.846	.630	7.56
abs. at 601 nm		.740	.551	7.57
abs. at 508 nm		.762	.563	7.75
abs. at 480 nm		.856	.636	7.62
Average Filtration Temp. = -38.0°C Solids = 9.3 wt% (Avg. of Both Dyes)				
mass, g	12.475	7.435	4.980	
density, g/mℓ		.827	.812	
abs. at 650 nm		.865	.652	9.32
abs. at 601 nm		.759	.574	9.22
abs. at 508 nm		.784	.589	9.42
abs. at 480 nm		.880	.663	9.33

Table XI

Method 2 Filtration and Dye Absorbance Data for LFP-3

	Initial Fuel	Filtrate	ΔA	Wt.% Solids
Average Filtration Temp. = -27.4°C Solids = 4.7 wt% (Avg. of Both Dyes)				
density, g/mℓ	.8176	.821		
abs. at 650 nm		.813	.043	4.95
abs. at 601 nm		.716	.037	4.82
abs. at 508 nm		.740	.036	4.52
abs. at 480 nm		.831	.039	4.35
Average Filtration Temp. = -28.0°C Solids = 4.5 wt% (Avg. of Both Dyes)				
density, g/mℓ	.8176	.822		
abs. at 650 nm		.815	.044	4.95
abs. at 601 nm		.717	.037	4.71
abs. at 508 nm		.739	.035	4.28
abs. at 480 nm		.829	.038	4.13
Average Filtration Temp. = -33.3°C Solids = 7.2 wt% (Avg. of Both Dyes)				
density, g/mℓ	.819	.823		
abs. at 650 nm		.846	.066	7.37
abs. at 601 nm		.741	.056	7.12
abs. at 508 nm		.765	.058	7.15
abs. at 480 nm		.856	.064	7.04

Table XI (continued)

Method 2 Filtration and Dye Absorbance Data for LFP-3

	Initial Fuel	Filtrate	ΔA	Wt.% Solids
Average Filtration Temp. = -37.9°C Solids = 9.3 wt% (Avg. of Both Dyes)				
density, g/mℓ	.820	.827		
abs. at 650 nm		.861	.087	9.43
abs. at 601 nm		.758	.075	9.22
abs. at 508 nm		.785	.078	9.26
abs. at 480 nm		.878	.086	9.12
Average Filtration Temp. = -42.8°C Solids = 12.0 wt% (Avg. of Both Dyes)				
density, g/mℓ	.818	.823		
abs. at 650 nm		.894	.113	12.08
abs. at 601 nm		.785	.097	11.79
abs. at 508 nm		.810	.103	12.15
abs. at 480 nm		.911	.113	11.84

Table XII

Method 1 Filtration and Dye Absorbance Data for LFP-5

	Initial Fuel	Filtrate	Precipitate	Wt.% Solids
Average Filtration Temp. = -33.8°C Solids = 2.3 wt% (Blue Dye Avg.)				
mass, g	12.588	10.046	2.516	
density, g/mℓ		.825	.818	
abs. at 650 nm		.816	.715	2.33
abs. at 601 nm		.715	.629	2.26
abs. at 508 nm		.708	.621	2.31
abs. at 480 nm		.793	.695	2.32
Average Filtration Temp. = -39.4°C Solids = 4.7 wt% (Blue Dye Avg.)				
mass, g	12.552	7.373	5.191	
density, g/mℓ		.825	.821	
abs. at 650 nm		.822	.726	4.64
abs. at 601 nm		.725	.640	4.66
abs. at 508 nm		.723	.633	4.96
abs. at 480 nm		.810	.709	4.97
Average Filtration Temp. = -44.4°C Solids = 5.8 wt% (Blue Dye Avg.)				
mass, g	12.711	6.446	6.199	
density, g/mℓ		.826	.818	
abs. at 650 nm		.838	.731	5.86
abs. at 601 nm		.739	.646	5.77
abs. at 508 nm		.738	.640	6.12
abs. at 480 nm		.828	.716	6.24

Table XIII

Method 2 Filtration and Dye Absorbance Data for LFP-5

	Initial Fuel	Filtrate	ΔA	Wt.% Solids
Average Filtration Temp. = -33.9°C Solids = 2.1 wt% (Blue Dye Avg.)				
density, g/mℓ	.822	.823		
abs. at 650 nm		.799	.0185	2.20
abs. at 601 nm		.705	.0145	1.94
abs. at 508 nm		.702	.0115	1.53
abs. at 480 nm		.787	.0125	1.48
Average Filtration Temp. = -39.3°C Solids = 5.1 wt% (Blue Dye Avg.)				
density, g/mℓ	.822	.825		
abs. at 650 nm		.826	.0445	5.05
abs. at 601 nm		.729	.040	5.15
abs. at 508 nm		.728	.042	5.43
abs. at 480 nm		.817	.0475	5.48
Average Filtration Temp. = -39.4°C Solids = 4.9 wt% (Blue Dye Avg.)				
density, g/mℓ	.822	.824		
abs. at 650 nm		.832	.043	4.87
abs. at 601 nm		.732	.0375	4.82
abs. at 508 nm		.729	.037	4.78
abs. at 480 nm		.818	.041	4.71
Average Filtration Temp. = -44.6°C Solids = 6.8 wt% (Blue Dye Avg.)				
density, g/mℓ	.823	.827		
abs. at 650 nm		.843	.062	6.80
abs. at 601 nm		.744	.054	6.70
abs. at 508 nm		.742	.0545	6.79
abs. at 480 nm		.831	.060	6.66

Table XIV

Method 1 Filtration and Dye Absorbance Data for NAPC-2

	Initial Fuel	Filtrate	Precipitate	Wt.% Solids
Average Filtration Temp. = -32.6°C Solids = 4.8 wt% (Blue Dye Avg.)				
mass, g	12.243	9.091	3.112	
density, g/mℓ		.831	.818	
abs. at 650 nm		.818	.653	4.81
abs. at 601 nm		.717	.573	4.79
abs. at 508 nm		.779	.609	5.24
abs. at 480 nm		.865	.652	5.97
Average Filtration Temp. = -34.6°C Solids = 6.6 wt% (Blue Dye Avg.)				
mass, g	12.624	8.490	4.120	
density, g/mℓ		.8323	.815	
abs. at 650 nm		.826	.644	6.65
abs. at 601 nm		.726	.567	6.61
abs. at 508 nm		.792	.605	7.18
abs. at 480 nm		.899	.662	8.09
Average Filtration Temp. = -37.6°C Solids = 8.0 wt% (Blue Dye Avg.)				
mass, g	12.989	7.329	5.637	
density, g/mℓ		.8333	.8196	
abs. at 650 nm		.840	.674	8.01
abs. at 601 nm		.738	.593	7.96
abs. at 508 nm		.808	.637	8.63
abs. at 480 nm		.920	.707	9.51
Average Filtration Temp. = -40.7°C Solids = 8.2 wt% (Blue Dye Avg.)				
mass, g	12.958	6.154	6.731	
density, g/mℓ		.8344	.8214	
abs. at 650 nm		.850	.704	8.28
abs. at 601 nm		.746	.619	8.20
abs. at 508 nm		.814	.662	9.08
abs. at 480 nm		.928	.739	9.98

Table XV

Method 2 Filtration and Dye Absorbance Data for NAPC-2

	Initial Fuel	Filtrate	ΔA	Wt.% Solids
Average Filtration Temp. = -29.5°C Solids = 2.8 wt% (Blue Dye Avg.)				
density, g/mℓ	.8273	.8295		
abs. at 650 nm	.770		.0255	2.95
abs. at 601 nm	.676		.020	2.62
abs. at 508 nm	.732		.021	2.53
abs. at 480 nm	.822		.0275	2.98
Average Filtration Temp. = -29.6°C Solids = 3.1 wt% (Blue Dye Avg.)				
density, g/mℓ	.8273	.8297		
abs. at 650 nm	.770		.0275	3.19
abs. at 601 nm	.676		.0225	2.97
abs. at 508 nm	.732		.0235	2.85
abs. at 480 nm	.822		.031	3.38
Average Filtration Temp. = -31.8°C Solids = 4.3 wt% (Blue Dye Avg.)				
density, g/mℓ	.8293	.8330		
abs. at 650 nm		.818	.040	4.47
abs. at 601 nm		.717	.033	4.18
abs. at 508 nm		.781	.035	4.06
abs. at 480 nm		.885	.044	4.56
Average Filtration Temp. = -32.6°C Solids = 5.2 wt% (Blue Dye Avg.)				
density, g/mℓ	.828	.832		
abs. at 650 nm	.770		.047	5.32
abs. at 601 nm	.676		.040	5.15
abs. at 508 nm	.732		.043	5.11
abs. at 480 nm	.822		.044	4.64

Table XV (continued)

Method 2 Filtration and Dye Absorbance Data for NAPC-2

	Initial Fuel	Filtrate	ΔA	Wt.% Solids
Average Filtration Temp. = -35.0°C Solids = 6.6 wt% (Blue Dye Avg.)				
density, g/mℓ	.828	.833		
abs. at 650 nm	.770		.0605	6.69
abs. at 601 nm	.676		.051	6.41
abs. at 508 nm	.732		.0555	6.45
abs. at 480 nm	.822		.0705	7.30
Average Filtration Temp. = -37.8°C Solids = 8.6 wt% (Blue Dye Avg.)				
density, g/mℓ	.828	.8340		
abs. at 650 nm	.770		.0795	8.69
abs. at 601 nm	.676		.0675	8.41
abs. at 508 nm	.732		.0785	9.02
abs. at 480 nm	.822		.098	9.99
Average Filtration Temp. = -40.5°C Solids = 9.9 wt% (Blue Dye Avg.)				
density, g/mℓ	.8300	.8369		
abs. at 650 nm	.770		.094	10.14
abs. at 601 nm	.676		.0785	9.66
abs. at 508 nm	.732		.088	9.99
abs. at 480 nm	.822		.116	11.64

Table XV (continued)

Method 2 Filtration and Dye Absorbance Data for NAPC-2

	Initial Fuel	Filtrate	ΔA	Wt.% Solids
Average Filtration Temp. = -40.7°C Solids = 8.1 wt% (Blue Dye Avg.)				
density, g/mℓ	.8273	.8342		
abs. at 650 nm	.770		.077	8.34
abs. at 601 nm	.676		.0635	7.83
abs. at 508 nm	.732		.0695	7.91
abs. at 480 nm	.822		.0905	9.17
Average Filtration Temp. = -41.7°C Solids = 9.2 wt% (Blue Dye Avg.)				
density, g/mℓ	.8305	.8380		
abs. at 650 nm		.861	.087	9.29
abs. at 601 nm		.753	.074	9.01
abs. at 508 nm		.825	.084	9.36
abs. at 480 nm		.937	.109	10.83
Average Filtration Temp. = -41.7°C Solids = 9.0 wt% (Blue Dye Avg.)				
density, g/mℓ	.8305	.8382		
abs. at 650 nm		.868	.087	9.18
abs. at 601 nm		.757	.073	8.80
abs. at 508 nm		.823	.081	9.00
abs. at 480 nm		.938	.102	10.04

Table XVI

Method 2 Filtration and Dye Absorbance Data for NAPC-3

	Initial Fuel	Filtrate	ΔA	Wt.% Solids
Average Filtration Temp. = -38.2°C Solids = 1.0 wt% (Avg. of Both Dyes)				
density, g/mℓ	.8140	.8139		
abs. at 650 nm		.752	.011	1.47
abs. at 601 nm		.664	.008	1.21
abs. at 508 nm		.691	.004	.59
abs. at 480 nm		.778	.005	.65
Average Filtration Temp. = -41.0°C Solids = 2.3 wt% (Avg. of Both Dyes)				
density, g/mℓ	.8141	.8151		
abs. at 650 nm		.768	.0225	2.81
abs. at 601 nm		.675	.0175	2.47
abs. at 508 nm		.700	.015	2.02
abs. at 480 nm		.790	.0165	1.96
Average Filtration Temp. = -41.7°C Solids = 2.6 wt% (Avg. of Both Dyes)				
density, g/mℓ	.8141	.8156		
abs. at 650 nm		.767	.025	3.08
abs. at 601 nm		.677	.020	2.78
abs. at 508 nm		.703	.018	2.38
abs. at 480 nm		.792	.020	2.35
Average Filtration Temp. = -44.7°C Solids = 3.9 wt% (Avg. of Both Dyes)				
density, g/mℓ	.8104	.8127		
abs. at 650 nm	.749		.036	4.32
abs. at 601 nm	.661		.030	4.08
abs. at 508 nm	.689		.028	3.64
abs. at 480 nm	.777		.031	3.57

Table XVI (continued)

Method 2 Filtration and Dye Absorbance Data for NAPC-3

	Initial Fuel	Filtrate	ΔA	Wt.% Solids
Average Filtration Temp. = -47.6°C Solids = 4.7 wt% (Avg. of Both Dyes)				
density, g/mℓ	.8104	.8132		
abs. at 650 nm	.749		.0435	5.17
abs. at 601 nm	.661		.036	4.84
abs. at 508 nm	.689		.034	4.38
abs. at 480 nm	.777		.037	4.22
Average Filtration Temp. = -50.4°C Solids = 6.2 wt% (Avg. of Both Dyes)				
density, g/mℓ	.8104	.8140		
abs. at 650 nm	.749		.058	6.78
abs. at 601 nm	.661		.048	6.36
abs. at 508 nm	.689		.046	5.85
abs. at 480 nm	.777		.051	5.75
Average Filtration Temp. = -52.4°C Solids = 6.2 wt% (Avg. of Both Dyes)				
density, g/mℓ	.8102	.8141		
abs. at 650 nm	.749		.057	6.63
abs. at 601 nm	.661		.048	6.33
abs. at 508 nm	.689		.048	6.07
abs. at 480 nm	.777		.052	5.83

Table XVI (continued)

Method 2 Filtration and Dye Absorbance Data for NAPC-3

	Initial Fuel	Filtrate	ΔA	Wt.% Solids
Average Filtration Temp. = -54.1°C Solids = 6.9 wt% (Avg. of Both Dyes)				
density, g/mℓ	.8102	.8146		
abs. at 650 nm	.749		.064	7.38
abs. at 601 nm	.661		.054	7.06
abs. at 508 nm	.689		.054	6.77
abs. at 480 nm	.777		.059	6.56
Average Filtration Temp. = -55.4°C Solids = 7.3 wt% (Avg. of Both Dyes)				
density, g/mℓ	.8102	.8152		
abs. at 650 nm	.749		.068	7.76
abs. at 601 nm	.661		.057	7.37
abs. at 508 nm	.689		.058	7.20
abs. at 480 nm	.777		.063	6.93
Average Filtration Temp. = -56.9°C Solids = 8.1 wt% (Avg. of Both Dyes)				
density, g/mℓ	.8117	.8169		
abs. at 650 nm	.749		.0745	8.47
abs. at 601 nm	.661		.064	8.25
abs. at 508 nm	.689		.064	7.92
abs. at 480 nm	.777		.070	7.68

Table XVII

Method 2 Filtration and Dye Absorbance Data for NAPC-5

	Initial Fuel	Filtrate	ΔA	Wt.% Solids
Average Filtration Temp. = -53.6°C Solids = 1.6 wt% (Blue Dye Avg.)				
density, g/mℓ	.8094	.8095		
abs. at 650 nm	.724		.013	1.75
abs. at 601 nm	.639		.010	1.53
abs. at 508 nm	.689		.0075	1.07
abs. at 480 nm	.784		.008	1.00
Average Filtration Temp. = -57.1°C Solids = 2.8 wt% (Blue Dye Avg.)				
density, g/mℓ	.8094	.8099		
abs. at 650 nm	.724		.023	3.01
abs. at 601 nm	.639		.0175	2.60
abs. at 508 nm	.689		.0155	2.13
abs. at 480 nm	.784		.0175	2.12
Average Filtration Temp. = -59.2°C Solids = 3.5 wt% (Blue Dye Avg.)				
density, g/mℓ	.8112	.8134		
abs. at 650 nm	.724		.030	3.72
abs. at 601 nm	.639		.023	3.21
abs. at 508 nm	.689		.0215	2.76
abs. at 480 nm	.784		.0245	2.77

Table XVII (continued)

Method 2 Filtration and Dye Absorbance Data for NAPC-5

	Initial Fuel	Filtrate	ΔA	Wt.% Solids
Average Filtration Temp. = -61.5°C Solids = 3.9 wt% (Blue Dye Avg.)				
density, g/mℓ	.8112	.8135		
abs. at 650 nm	.724		.0335	4.15
abs. at 601 nm	.639		.0265	3.71
abs. at 508 nm	.689		.0255	3.29
abs. at 480 nm	.784		.0285	3.23
Average Filtration Temp. = -64.8°C Solids = 4.8 wt% (Blue Dye Avg.)				
density, g/mℓ	.8112	.8142		
abs. at 650 nm	.724		.041	5.01
abs. at 601 nm	.639		.033	4.56
abs. at 508 nm	.689		.032	4.08
abs. at 480 nm	.784		.036	4.03
Average Filtration Temp. = -68.1°C Solids = 5.5 wt% (Blue Dye Avg.)				
density, g/mℓ	.8112	.8143		
abs. at 650 nm	.724		.0475	5.79
abs. at 601 nm	.639		.038	5.25
abs. at 508 nm	.689		.0375	4.79
abs. at 480 nm	.784		.042	4.72

Table XVIII

Method 2 Filtration and Dye Absorbance Data for LFPA-3

	Initial Fuel	Filtrate	ΔA	Wt.% Solids
Average Filtration Temp. = -45.8°C Solids = 2.5 wt% (Avg. of Both Dyes)				
density, g/mℓ	.7926	.7942		
abs. at 650 nm	.744		.025	3.07
abs. at 601 nm	.652		.019	2.65
abs. at 508 nm	.663		.0155	2.10
abs. at 480 nm	.752		.017	2.02
Average Filtration Temp. = -49.3°C Solids = 5.3 wt% (Avg. of Both Dyes)				
density, g/mℓ	.7926	.7955		
abs. at 650 nm	.744		.047	5.61
abs. at 601 nm	.652		.039	5.31
abs. at 508 nm	.663		.0385	5.15
abs. at 480 nm	.752		.043	5.07
Average Filtration Temp. = -51.3°C Solids = 8.0 wt% (Avg. of Both Dyes)				
density, g/mℓ	.7926	.7961		
abs. at 650 nm	.744		.074	8.65
abs. at 601 nm	.652		.0615	8.22
abs. at 508 nm	.663		.0585	7.70
abs. at 480 nm	.752		.065	7.55
Average Filtration Temp. = -52.0°C Solids = 8.7 wt% (Avg. of Both Dyes)				
density, g/mℓ	.7926	.7963		
abs. at 650 nm	.744		.076	8.85
abs. at 601 nm	.652		.0655	8.71
abs. at 508 nm	.663		.066	8.64
abs. at 480 nm	.752		.074	8.54

Table XVIII (continued)

Method 2 Filtration and Dye Absorbance Data for LFPA-3

	Initial Fuel	Filtrate	ΔA	Wt.% Solids
Average Filtration Temp. = -53.3°C Solids = 10.2 wt% (Avg. of Both Dyes)				
density, g/mℓ	.7926	.7973		
abs. at 650 nm	.744		.093	10.58
abs. at 601 nm	.652		.0795	10.34
abs. at 508 nm	.663		.0785	10.06
abs. at 480 nm	.752		.0875	9.89
Average Filtration Temp. = -55.3°C Solids = 11.9 wt% (Avg. of Both Dyes)				
density, g/mℓ	.7926	.7993		
abs. at 650 nm	.744		.109	12.05
abs. at 601 nm	.652		.094	11.87
abs. at 508 nm	.663		.0955	11.86
abs. at 480 nm	.752		.1065	11.67
Average Filtration Temp. = -58.2°C Solids = 14.3 wt% (Avg. of Both Dyes)				
density, g/mℓ	.7926	.8009		
abs. at 650 nm	.744		.134	14.38
abs. at 601 nm	.652		.1155	14.17
abs. at 508 nm	.663		.119	14.34
abs. at 480 nm	.752		.1335	14.19
Average Filtration Temp. = -60.3°C Solids = 16.7 wt% (Avg. of Both Dyes)				
density, g/mℓ	.7926	.8008		
abs. at 650 nm	.744		.1575	16.62
abs. at 601 nm	.652		.1375	16.57
abs. at 508 nm	.663		.143	16.90
abs. at 480 nm	.752		.161	16.79

Table XIX

Wt% Precipitate and Wt% Recovery
for Method 1 Filtration Experiments

Fuel ID	T, °C	% recovery	%P	%S
Fuel #7	-33.9	99.7	6.9	1.7
	-39.2	99.8	11.0	3.5
	-39.2	99.8	11.7	3.8
	-44.1	99.8	13.3	5.5
	-44.1	99.9	13.5	5.6
	-49.1	99.8	18.2	6.7
	-49.3	99.7	18.4	6.7
	-54.2	99.6	31.0	8.2
Shale II JP-5	-52.6	99.8	9.5	2.9±0.1
	-52.6	99.6	10.6	3.1±0.1
	-52.4	99.6	9.8	2.8±0.1
	-52.7	99.4	10.1	2.9±0.1
	-54.4	99.2	13.1	4.0±0.1
	-54.3	99.0	13.8	4.4±0.2
	-56.3	99.5	19.5	6.1±0.2
	-57.1	98.9	21.9	5.6±0.2
	-56.8	97.6	25.1	5.1±0.2
LFP-3	-23.1	99.7	12.9	2.9±0.1
	-27.2	99.7	15.8	5.0±0.1
	-27.7	99.6	15.8	4.7±0.1
	-33.2	99.9	31.2	7.6±0.3
	-38.0	99.5	40.1	9.3±0.4
LFP-5	-33.8	99.8	20.0	2.3±0.2
	-39.2	100	41.3	4.7±0.5
	-44.4	99.5	49.0	5.8±0.5
NAPC-2	-32.6	99.7	25.5	4.8±0.3
	-34.6	99.9	32.7	6.6±0.3
	-37.6	99.8	43.5	8.0±0.4
	-40.7	99.4	52.2	8.2±0.5

Table XX

Fuel Pour Properties

Fuel ID	Equilibrium Pour Pt., °C	Wt.% Solid at Pour Pt.
LFP-3	-27	4.7
LFP-5	-36	3.4
Fuel #7	-52	7.7
LFPA-3	-47	3.5
Shale II JP-5	-53	3.0
NAPC-2	-30	3.2
NAPC-3	-41	2.3
NAPC-5	-57	2.8

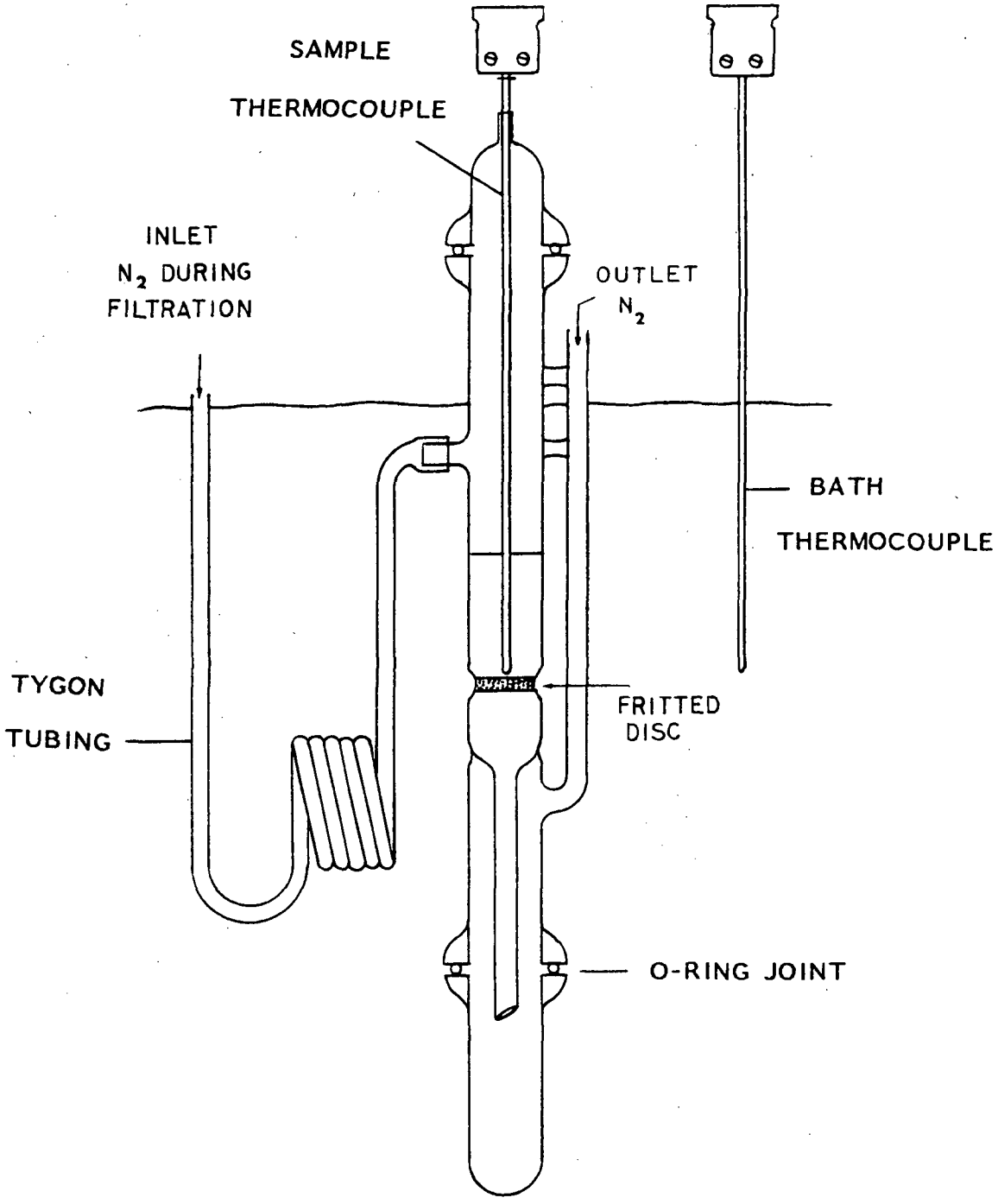

Figure 1: Schematic of the Liquid-Solid-Separator.

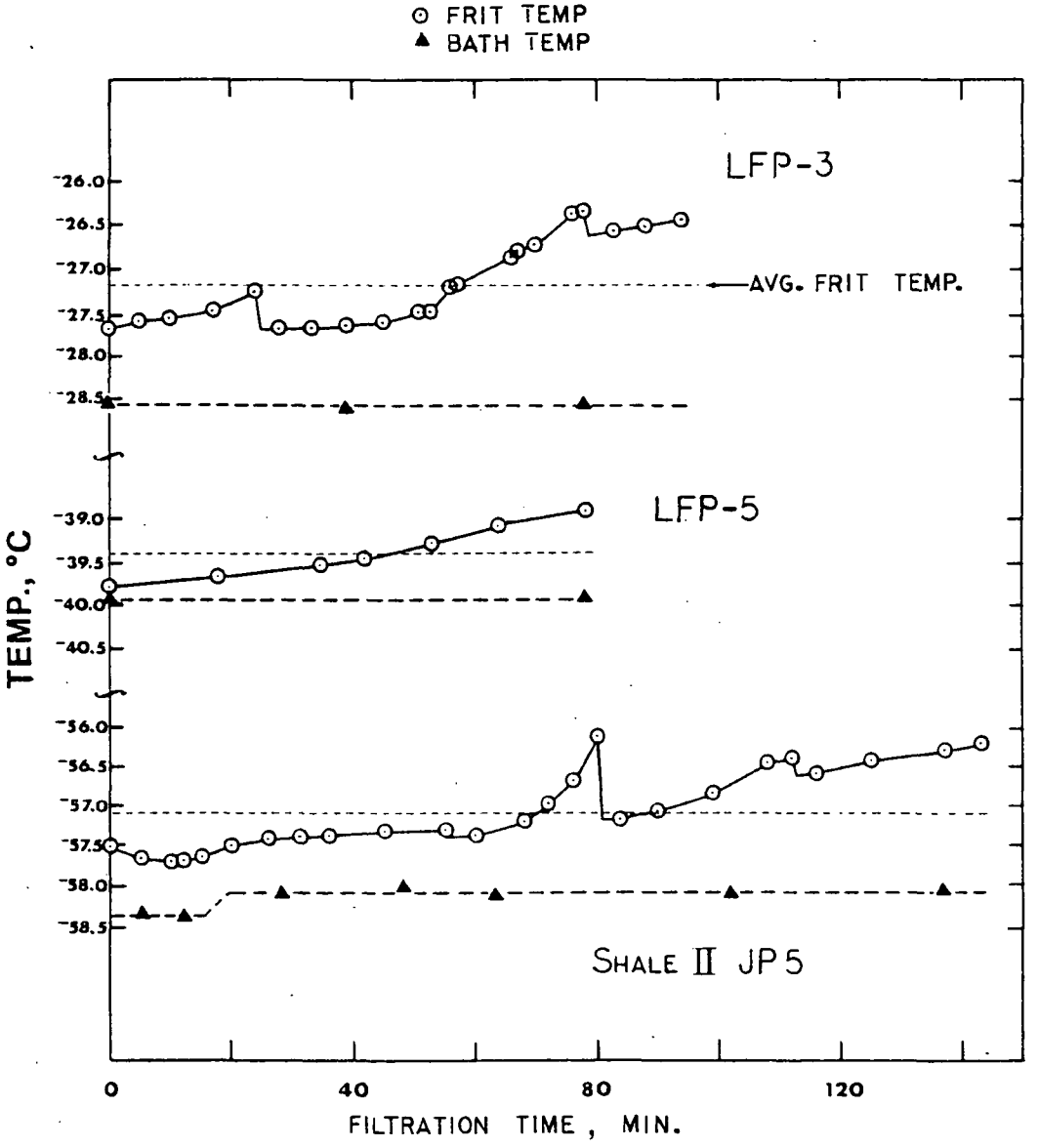

Figure 2: Frit and Bath Temperatures During Filtration.

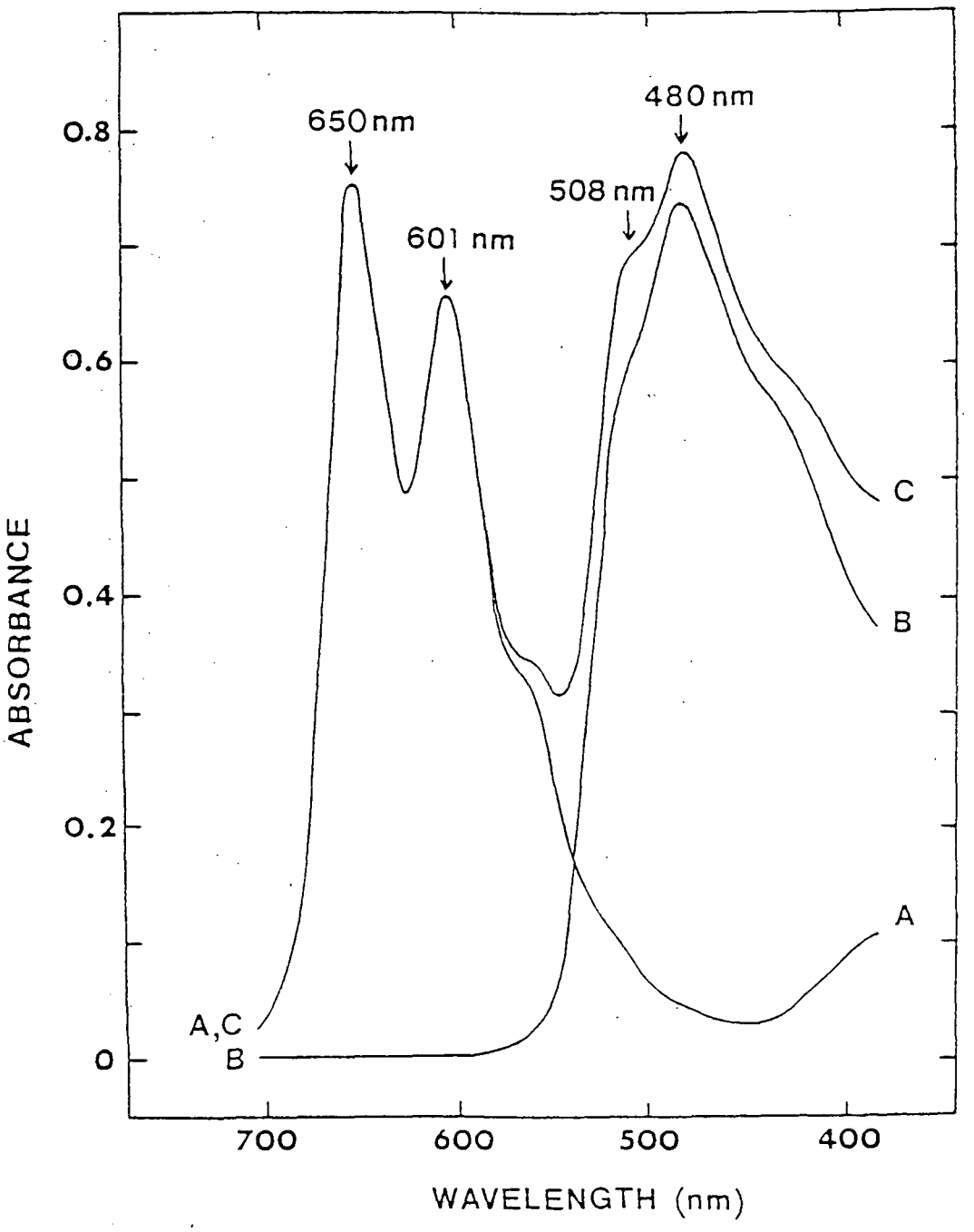

Figure 3: Spectra of Initial Fuel Containing (A) 60 ppm Blue Dye, (B) 40 ppm Orange Dye, (C) 100 ppm Total.

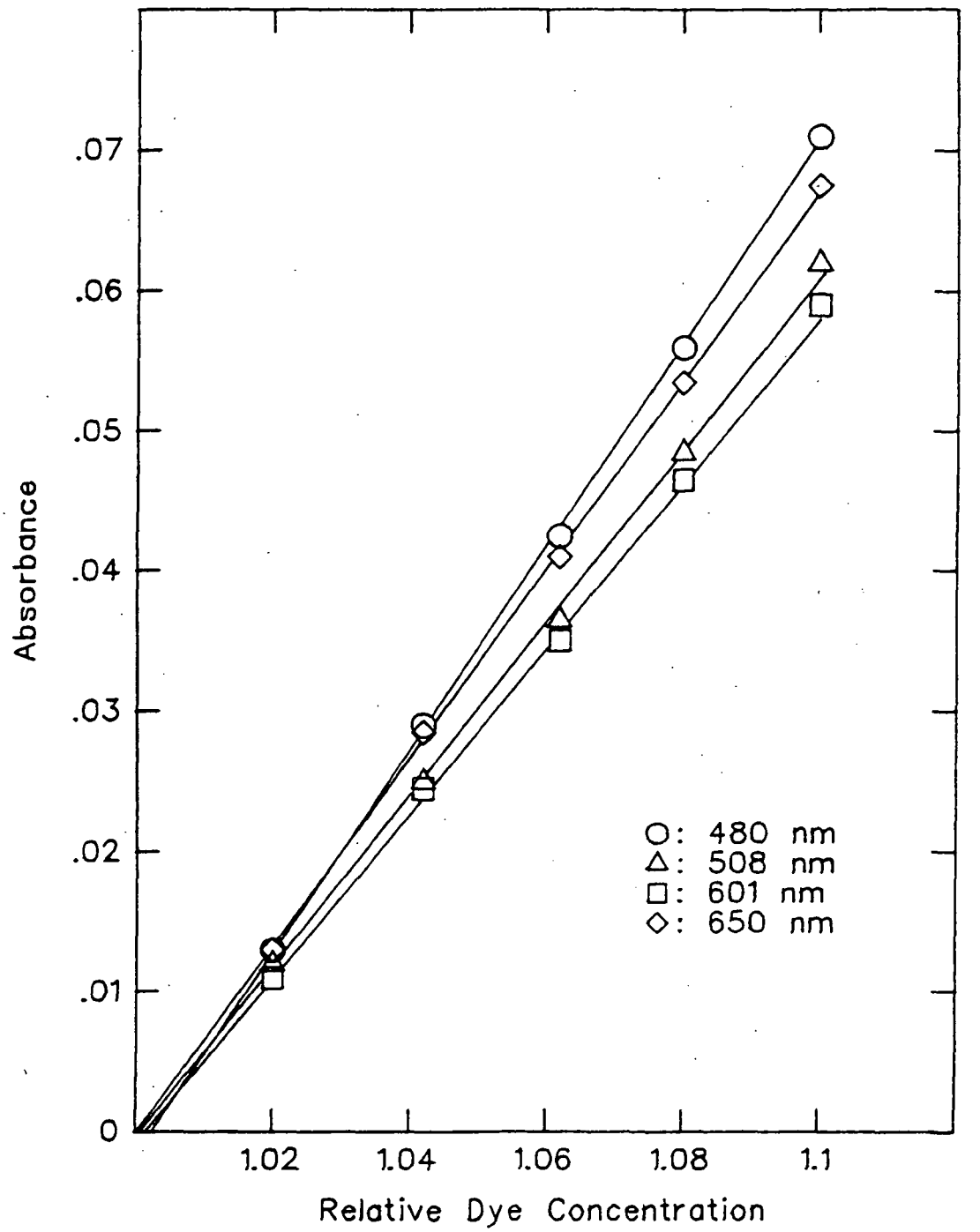

Figure 4: NAPC-5 Absorbance vs. Dye Concentration.

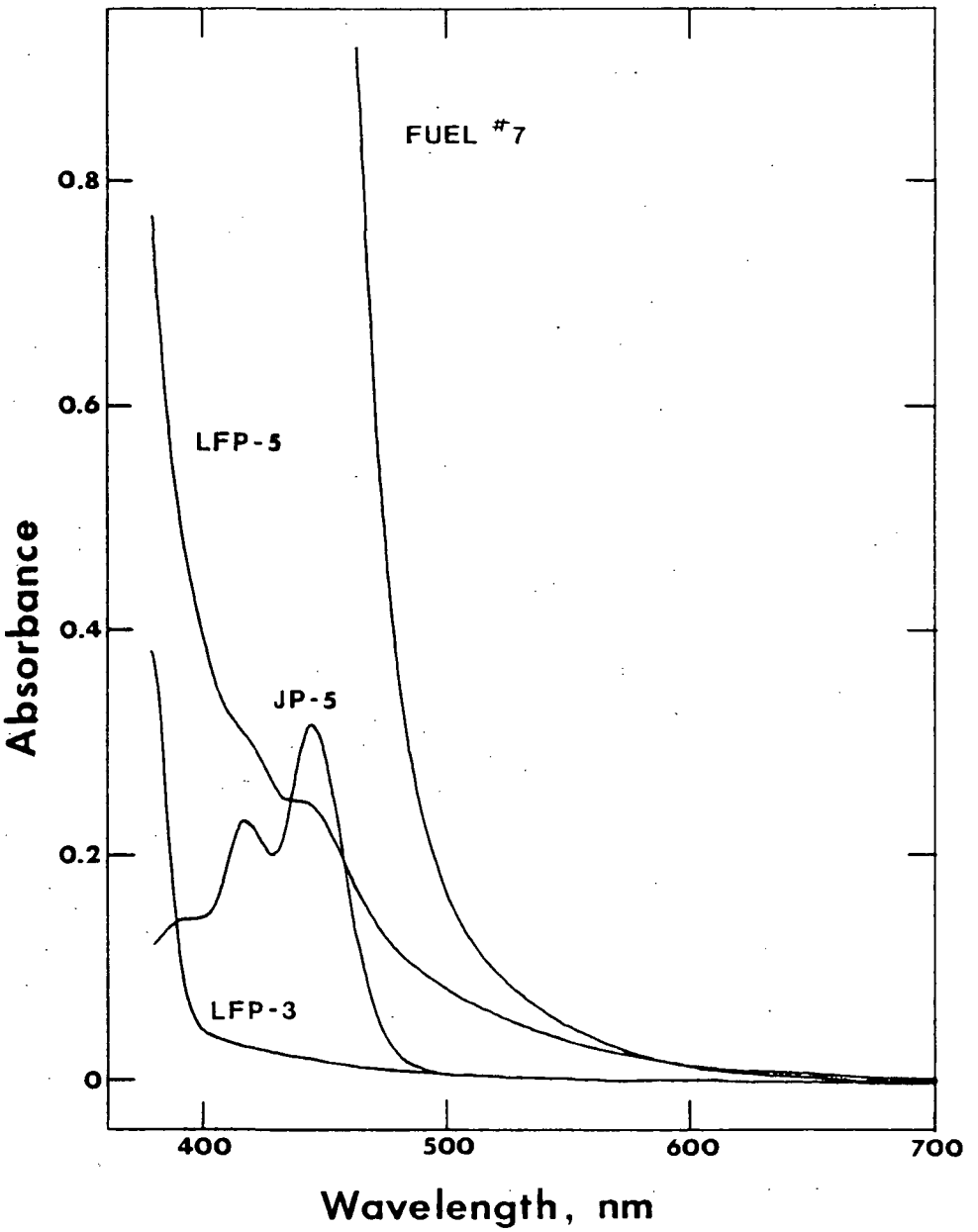

Figure 5: Original Fuel Absorbance Spectra.

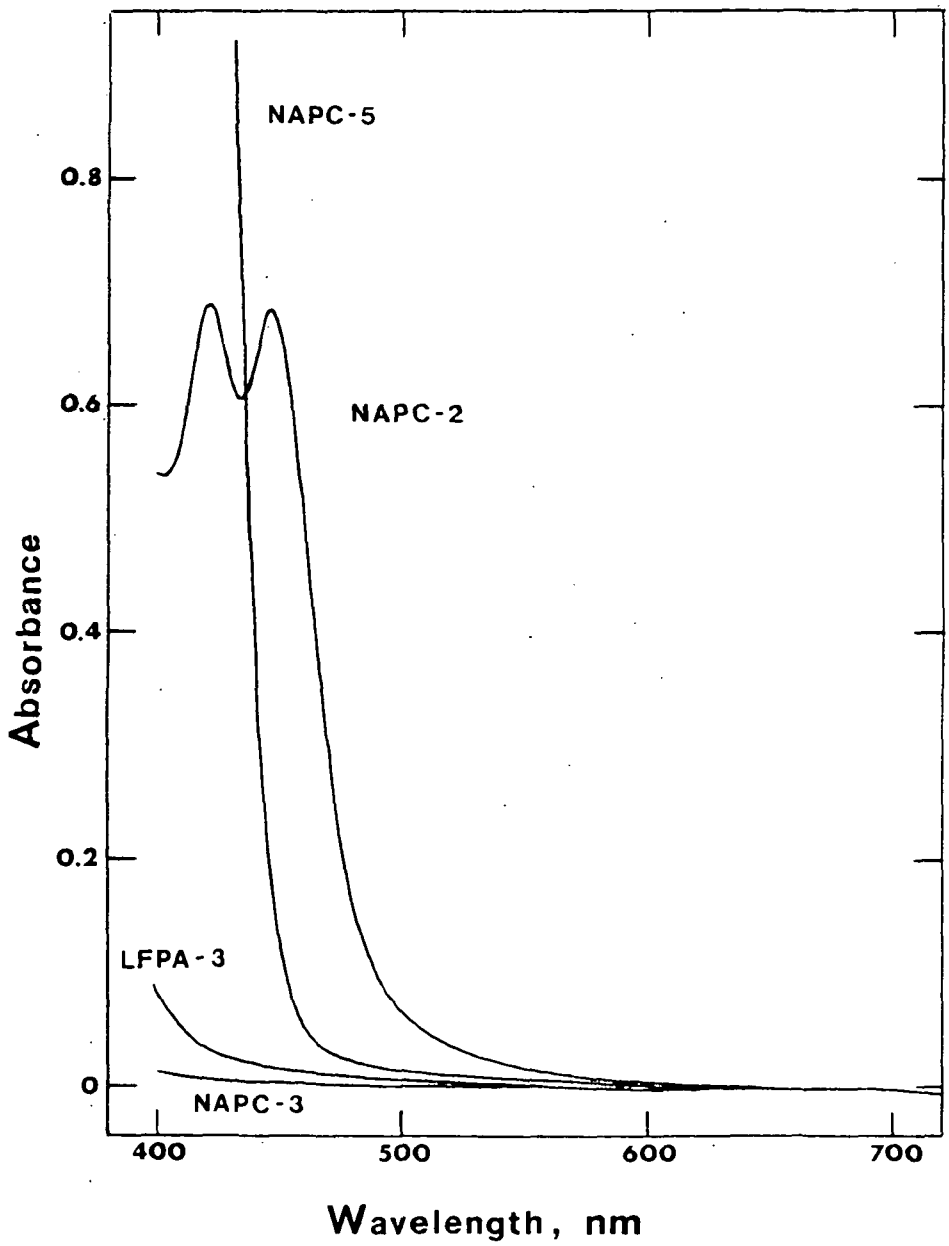

Figure 6: Original Fuel Absorbance Spectra.

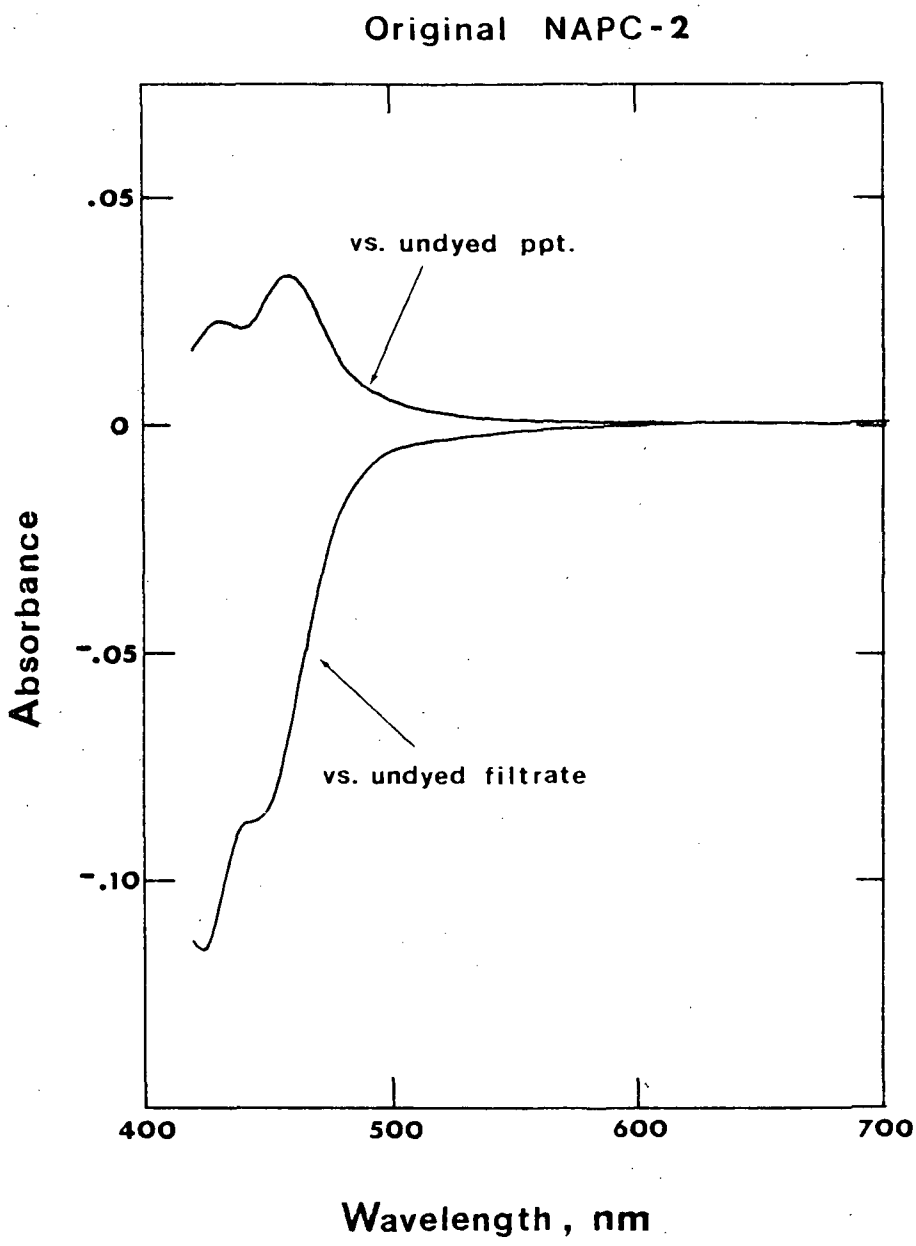

Figure 7: Undyed NAPC-2 Absorbance Compared to Its Separated Fractions.

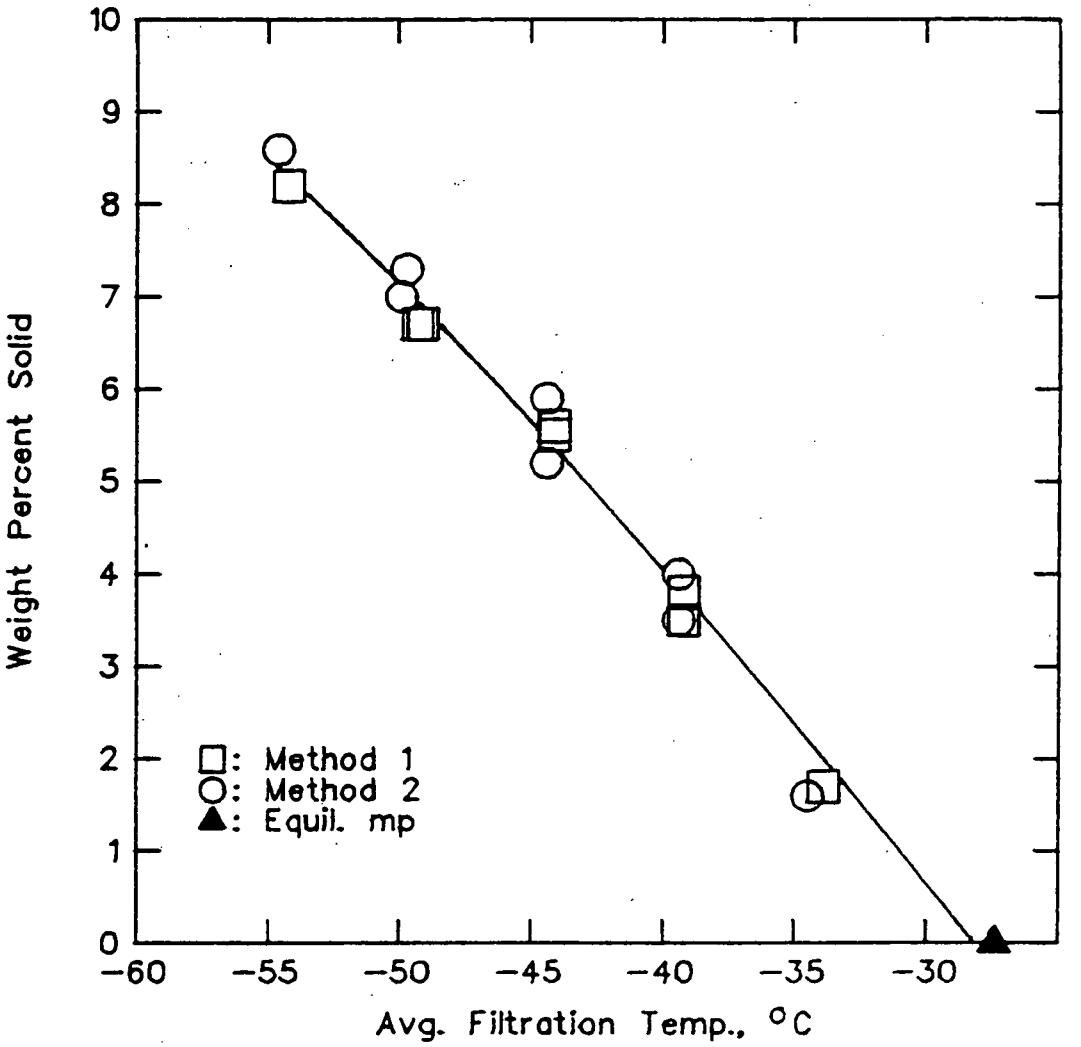

Figure 8: Fuel #7 Wt% Solid vs. Temperature.

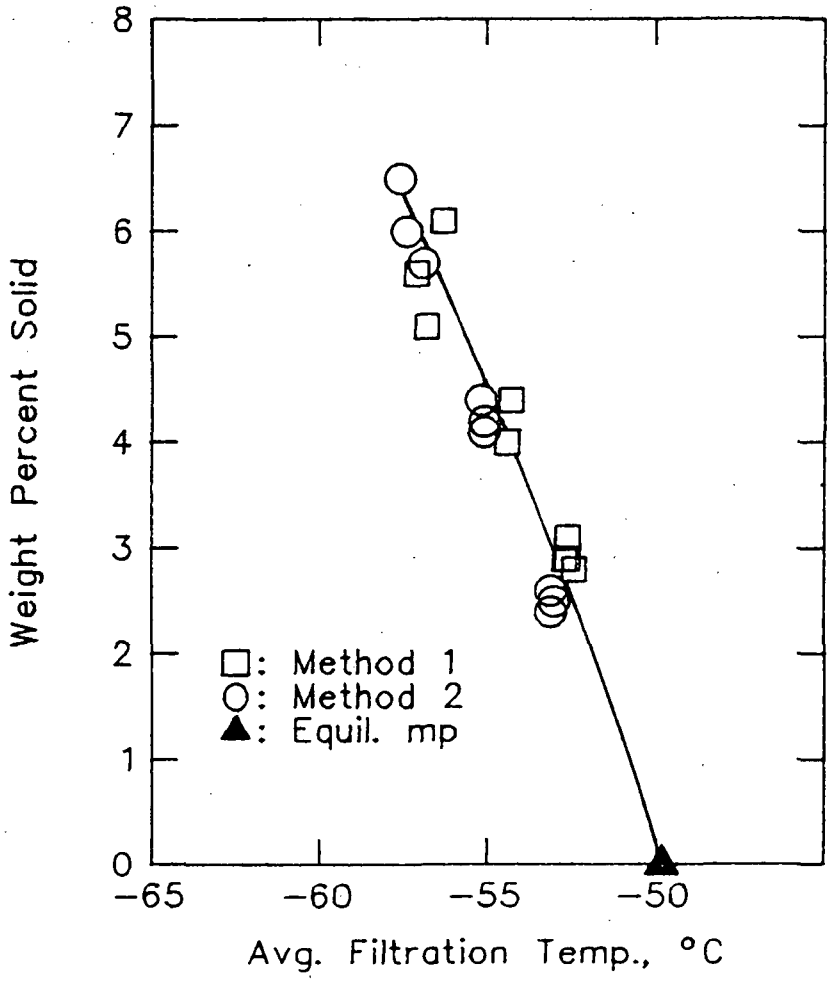

Figure 9: Shale II JP-5 Wt% Solid vs. Temperature.

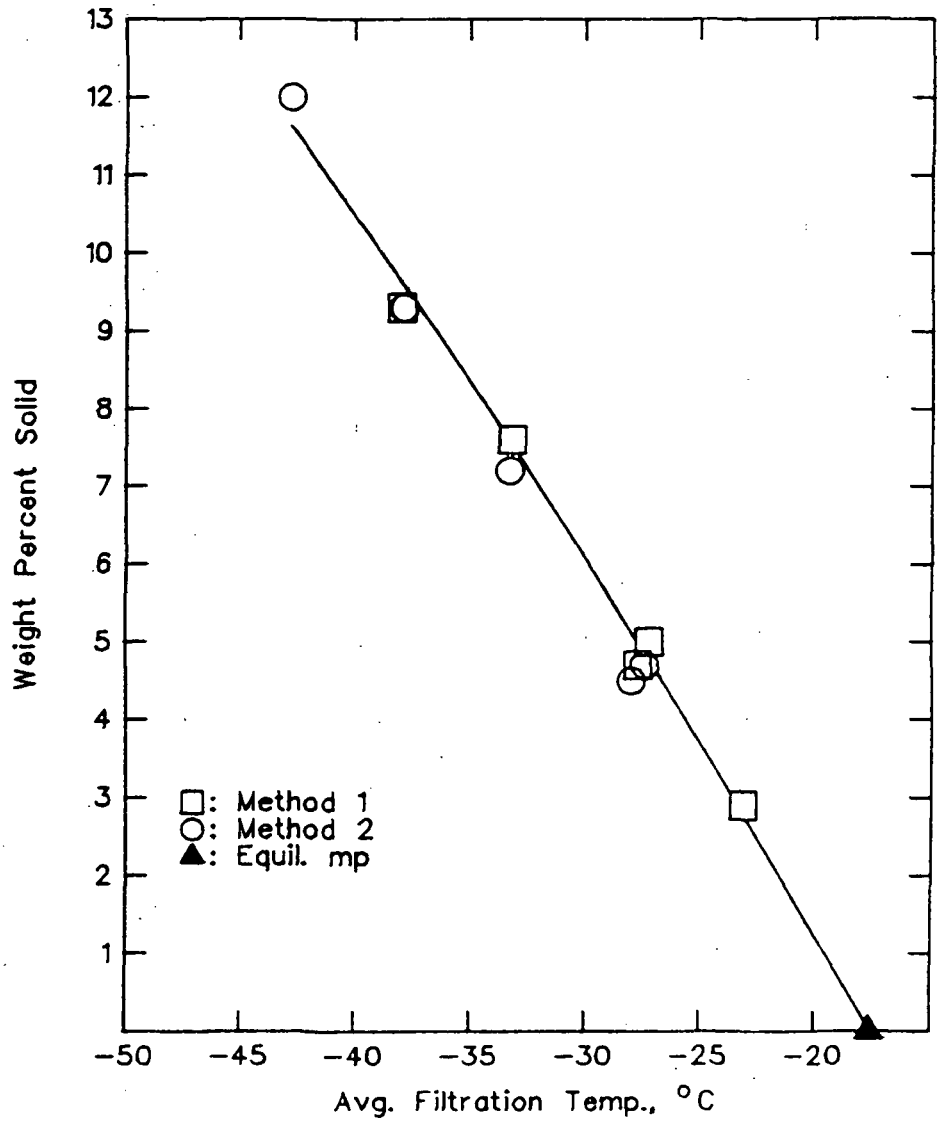

Figure 10: LFP-3 Wt% Solid vs. Temperature.

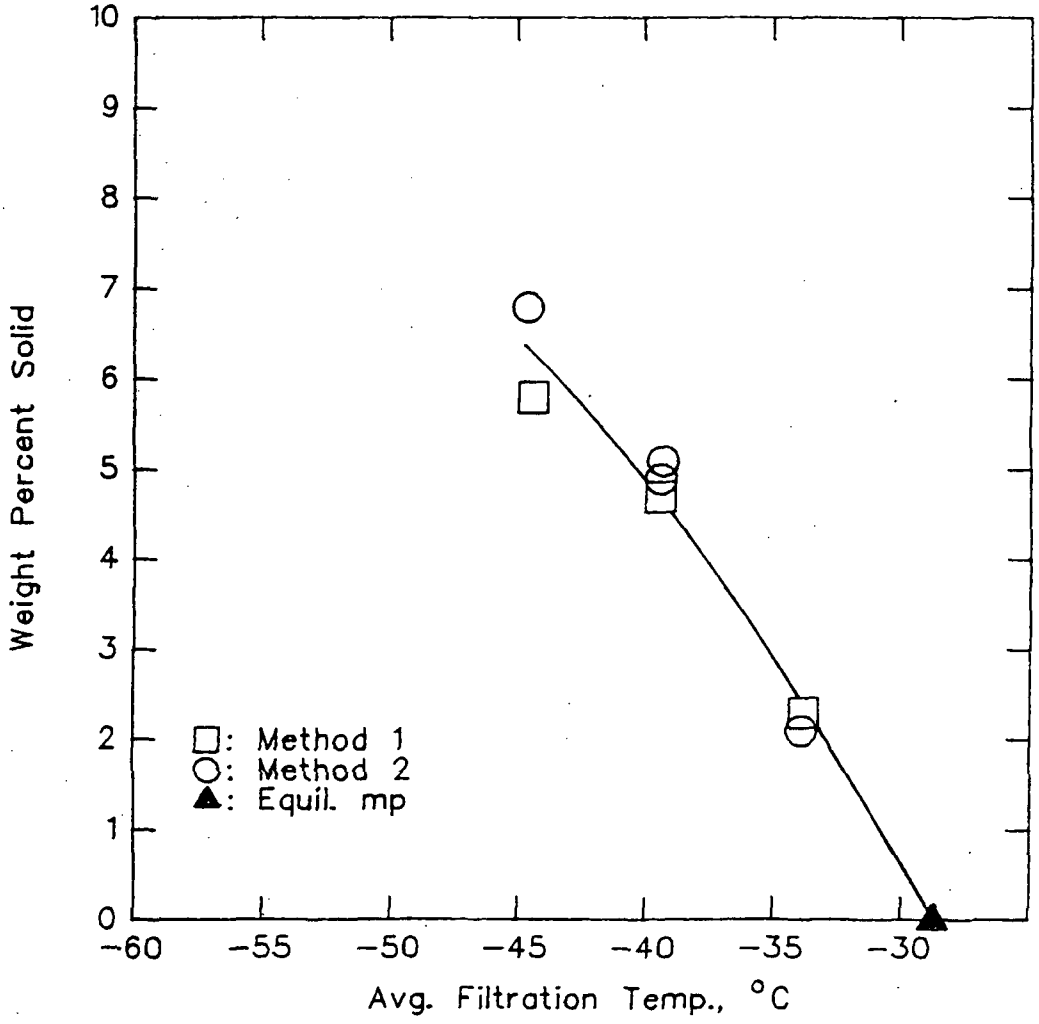

Figure 11: LFP-5 Wt% Solid vs. Temperature.

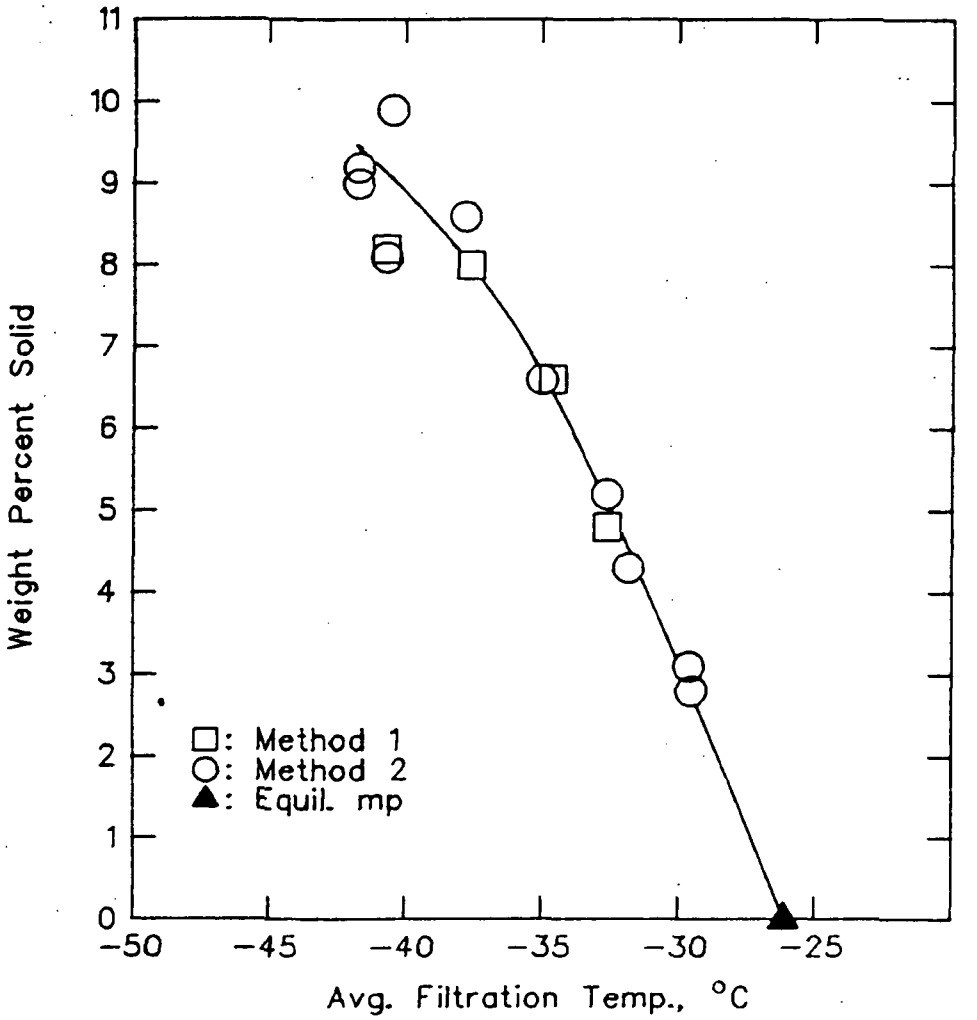

Figure 12: NAPC-2 Wt% Solid vs. Temperature.

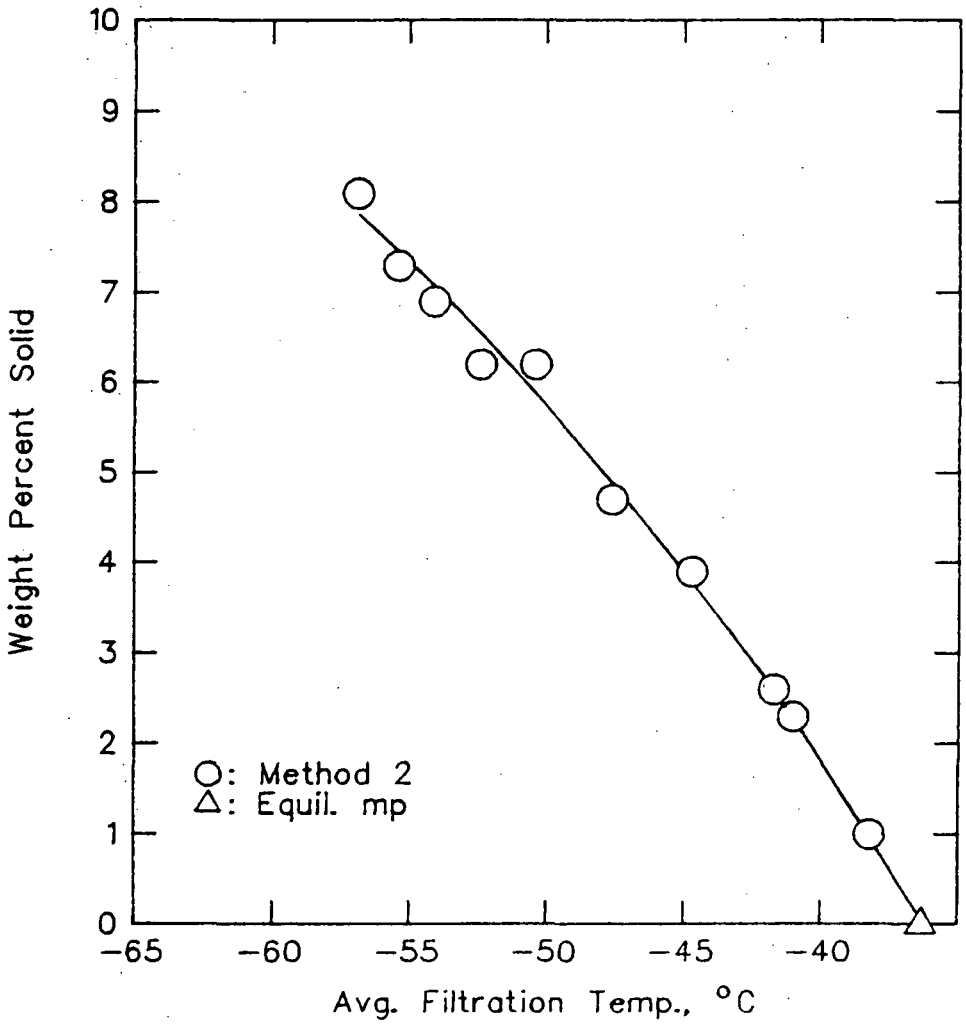

Figure 13: NAPC-3 Wt% Solid vs. Temperature.

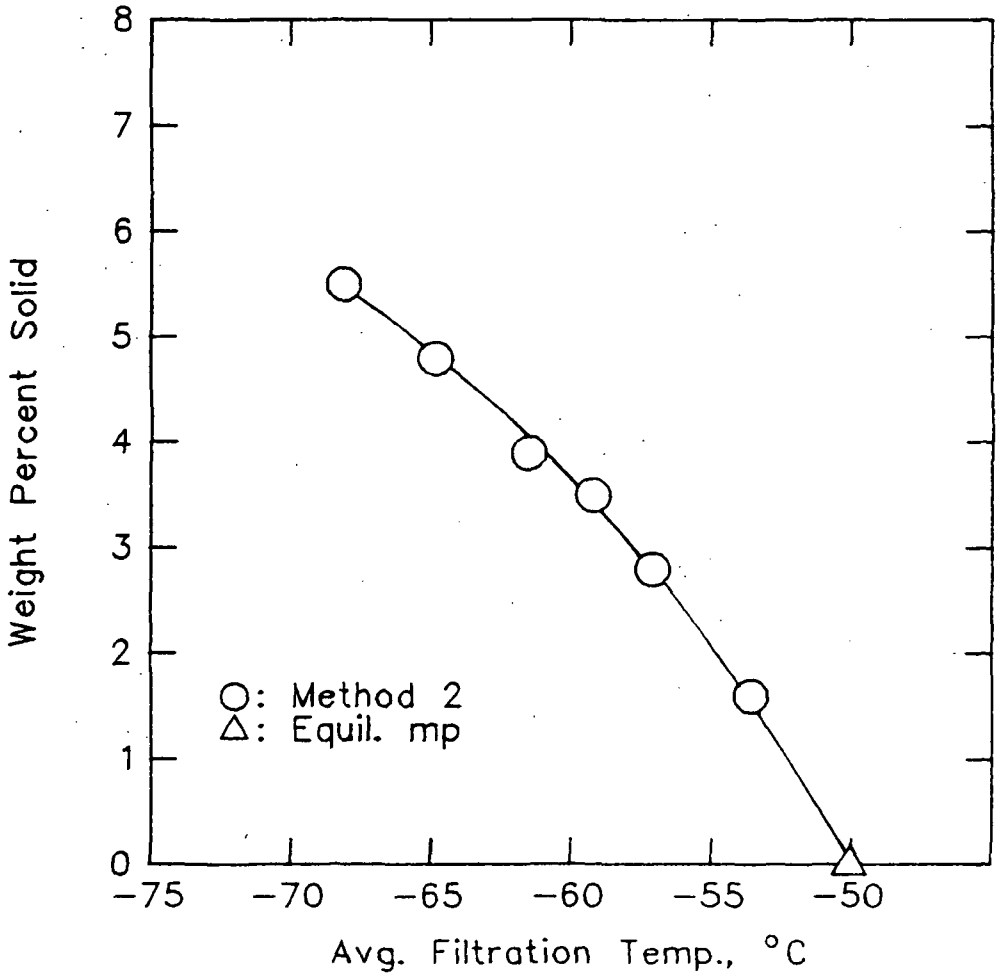

Figure 14: NAPC-5 Wt% Solid vs. Temperature.

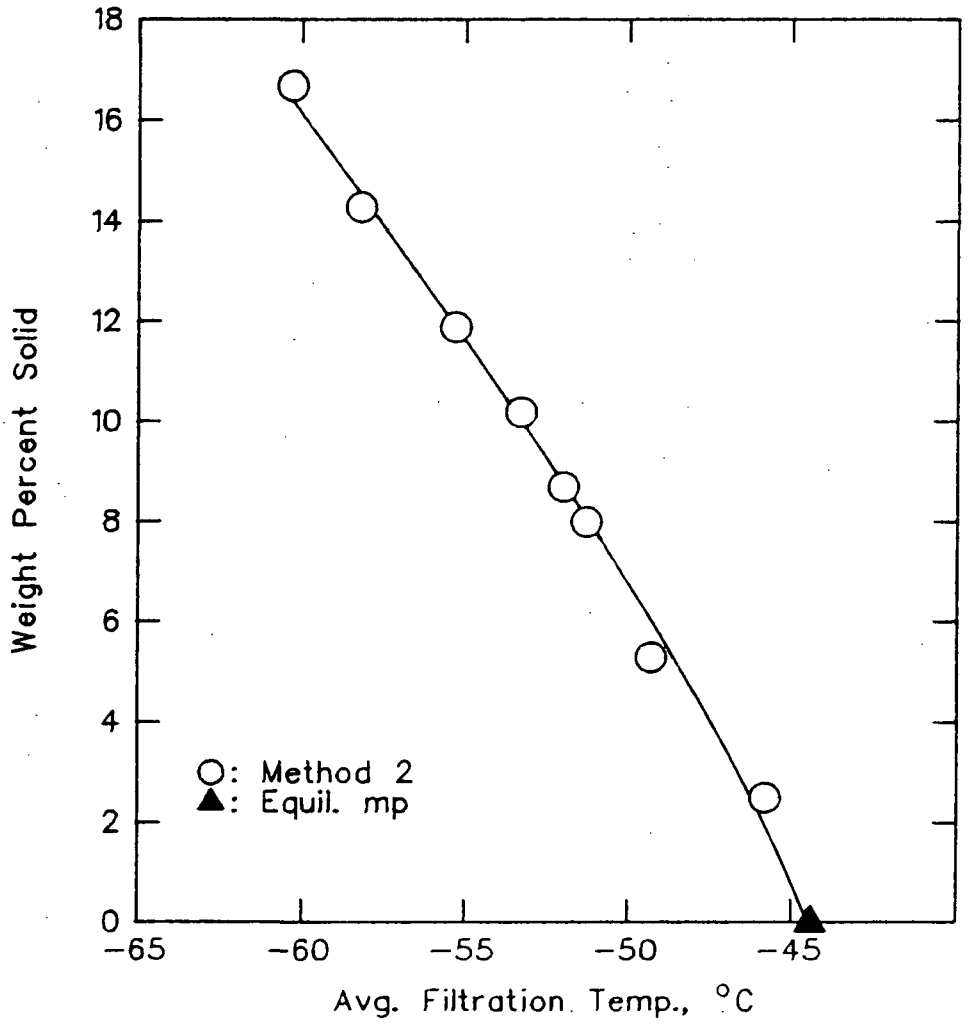

Figure 15: LFPA-3 Wt% Solid vs. Temperature.

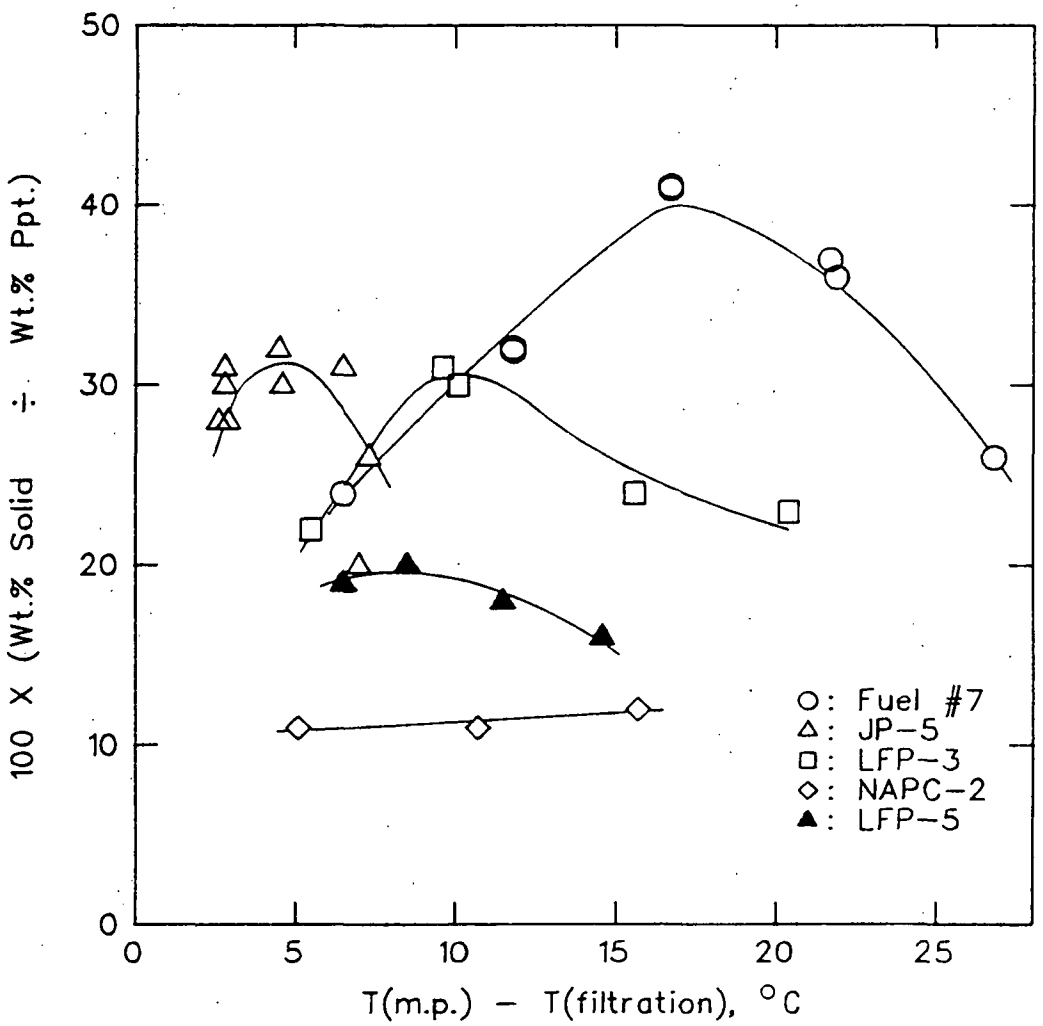

Figure 16: Wt% Solid in Precipitate Fraction vs. °C Below the Melting Point.

1. Report No.	2. Government Accession No.	3. Recipient's Catalog No.
NASA CR-179472		

4. Title and Subtitle	5. Report Date
Determination of Solid Mass Fraction in Partially Frozen Hydrocarbon Fuels	July 1986
	6. Performing Organization Code

7. Author(s)	8. Performing Organization Report No.
E.M. Cotterell, R. Mossadegh, A.J. Bruce and C.T. Moynihan	
	10. Work Unit No.

9. Performing Organization Name and Address	11. Contract or Grant No.
Rensselaer Polytechnic Institute Materials Engineering Department Troy, New York 12180-3590	NAG 3-213
	13. Type of Report and Period Covered
12. Sponsoring Agency Name and Address	Contractor Report
National Aeronautics and Space Administration Washington, D.C. 20546	14. Sponsoring Agency Code 505-31-42

15. Supplementary Notes

Final report. Project Manager, Robert Friedman, Aeropropulsion Facilities and Experiments Division, NASA Lewis Research Center, Cleveland, Ohio 44135.

16. Abstract

Filtration procedures alone are insufficient to determine the amounts of crystalline solid in a partially frozen hydrocarbon distillate fraction. This is due to the nature of the solidification process by which a large amount of liquid becomes entrapped within an interconnected crystalline structure. A technique has been developed to supplement filtration methods with an independent determination of the amount of liquid in the precipitate thereby revealing the actual value of mass percent crystalline solid, %S. A non-crystallizing dye is injected into the fuel and used as a tracer during the filtration. The relative concentrations of the dye in the filtrate and precipitate fractions is subsequently detected by a spectrophotometric comparison. The filtration apparatus was assembled so that the temperature of the sample is recorded immediately above the filter. Also, a second method of calculation has been established which allows significant reduction in test time while retaining acceptable accuracy of results. Data have been obtained for eight different kerosene range hydrocarbon fuels.

17. Key Words (Suggested by Author(s))	18. Distribution Statement
Fuels; Jet fuels; Hydrocarbon fuels; Freezing point; Crystallization; Filtration	Unclassified - unlimited STAR Category 28

19. Security Classif. (of this report)	20. Security Classif. (of this page)	21. No. of pages	22. Price*
Unclassified	Unclassified	89	A05

*For sale by the National Technical Information Service, Springfield, Virginia 22161